Journal of Drug Delivery Science and Technology 122 (2026) 108388

Contents lists available at ScienceDirect

Journal of Drug Delivery Science and Technology

journal homepage: www.elsevier.com/locate/jddst

Intranasal delivery of a nanoencapsulated ursodeoxycholic acid-ferulic acid prodrug enables CNS exposure to antioxidant agents

Giada Botti [a], Elena Marchesi [a], Luca Ferraro [b], Sarah Beggiato [b], Anna Bianchi [a], Barbara Pavan [c,d,*], Catia Contado [a], Federico Spizzo [e], Lucia Del Bianco [e], Daniela Perrone [f], Alessandro Dalpiaz [a]

[a] Department of Chemical, Pharmaceutical and Agricultural Sciences, University of Ferrara, Via L. Borsari 46, Ferrara, I-44121, Italy
[b] Department of Life Sciences and Biotechnology and LTTA Center, University of Ferrara, Via L. Borsari 46, Ferrara, I-44121, Italy
[c] Department of Neurosciences and Rehabilitation – Section of Physiology, University of Ferrara, via L. Borsari 46, Ferrara, I-44121, Italy
[d] Center for Translational Neurophysiology of Speech and Communication (CTNSC), Italian Institute of Technology (IIT), via Fossato di Mortara 19, Ferrara, I-44121, Italy
[e] Department of Physics and Earth Science, University of Ferrara, via G. Saragat 1, Ferrara, I-44122, Italy
[f] Department of Environmental and Prevention Sciences, University of Ferrara, Via L. Borsari 46, Ferrara, I-44121, Italy

ARTICLE INFO

Keywords:
Ursodeoxycholic and ferulic acids
Prodrug
Antioxidant activity
Solid lipid nanoparticles
Nasal administration
Brain delivery

ABSTRACT

Ursodeoxycholic acid (UDCA) and ferulic acid (Fer) are recognized for their neuroprotective effects against oxidative stress, being antioxidant agents able to preserve cell mitochondrial functions. This makes them potentially useful for neuronal protection against neurodegenerative disorders. Consequently, a new prodrug (UDC-Fer-Me) was developed as an ester-conjugate of the methyl-derivative of ferulic acid (Fer-Me), which retains the antioxidant properties of Fer and UDCA. The prodrug was encapsulated in compritol-based solid lipid nanoparticles (SLNs) for its nasal administration and nose-to-brain delivery. HPLC measurements demonstrated that (*i*) UDC-Fer-Me is hydrolyzed in rat liver and brain homogenates, as well as following intravenous administration in rats, leading to the release of UDCA and Fer-Me; (*ii*) the prodrug is not detectable in the cerebrospinal fluid (CSF) after intravenous administration to rats; however, (*iii*) it permeates *in vitro* nasal mucosal cells, inducing its partial hydrolysis. UDC-Fer-Me also counteracted reactive oxygen species production induced by H_2O_2 on cultured neuronal cells. The UDC-Fer-Me-loaded SLNs showed a particle size distribution in the ~0.1 μm order of magnitude and markedly improved the very slow dissolution rate of the prodrug in aqueous environments. Differential scanning calorimetry measurements suggested a good dispersion of the prodrug within the lipid matrix of SLNs; the drug loading was about 8% (61% entrapment efficiency). Following nasal administration of SLNs to rats (2 mg/kg dose), both the prodrug and Fer-Me were detected in the CSF at concentrations reaching up to 2 μg/mL, consistent with drug delivery to the central nervous system following intranasal administration.

1. Introduction

It is well established that phytochemicals are emerging as complementary or alternative therapeutic agents capable of counteracting the development and progression of neurodegenerative disorders [1–6]. Among these, ferulic acid (Fer; Fig. 1) has been extensively investigated for its antioxidant activity in neuronal models [5] and has been shown to protect against mitochondrial dysfunction induced by reactive oxygen species (ROS) [6]. Such dysfunction leads to further ROS accumulation, ATP depletion, and energy failure, ultimately contributing to neurodegeneration [7].

Ursodeoxycholic acid (UDCA; Fig. 1) has also been reported to exert neuroprotective effects by preserving mitochondrial integrity and restoring mitochondrial dynamics under oxidative stress conditions [8].

This article is part of a special issue entitled: Skin and mucosal drug delivery published in Journal of Drug Delivery Science and Technology.

* Corresponding author. Neurosciences and Rehabilitation – Section of Physiology, University of Ferrara, Via L. Borsari 46, I-44121, Ferrara, Italy.
E-mail addresses: bttgdi@unife.it (G. Botti), mrclne@unife.it (E. Marchesi), frl@unife.it (L. Ferraro), bggsrh@unife.it (S. Beggiato), bna@unife.it (A. Bianchi), pvnbbr@unife.it (B. Pavan), kat@unife.it (C. Contado), federico.spizzo@unife.it (F. Spizzo), lucia.delbianco@unife.it (L. Del Bianco), prd@unife.it (D. Perrone), dla@unife.it (A. Dalpiaz).

https://doi.org/10.1016/j.jddst.2026.108388
Received 10 February 2026; Received in revised form 10 April 2026; Accepted 27 April 2026
Available online 29 April 2026
1773-2247/

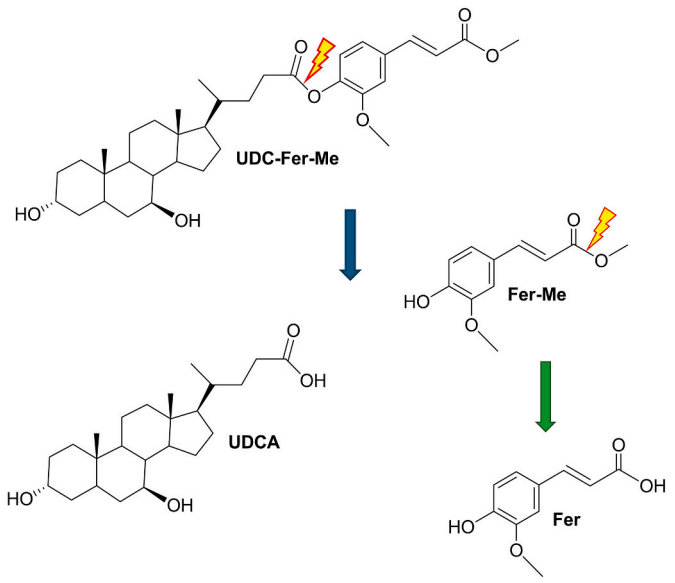

Fig. 1. Chemical structures of ursodeoxycholic acid (UDCA), ferulic acid (Fer), its methyl-ester methyl ferulate (Fer-Me), and the ester conjugate UDC-Fer-Me. The main sites of potential hydrolysis are indicated.

The ability of both Fer and UDCA to modulate mitochondrial function is particularly relevant in dopaminergic neurons of the substantia nigra pars compacta (SNpc), whose degeneration represents a hallmark of Parkinson's disease (PD). These neurons are characterized by high ROS production and increased vulnerability compared with dopaminergic neurons of the ventral tegmental area [9,10].

Although both Fer and UDCA can cross the blood-brain barrier (BBB) [11,12], their therapeutic application is limited by unfavorable pharmacokinetic properties, including suboptimal bioavailability and inefficient brain delivery following oral administration. As a consequence, very high oral doses (up to 50 mg/kg/day) are required to achieve neuroprotective effects in both humans and animal models [12–15].

Intranasal administration represents a promising non-invasive alternative route for drug delivery to the central nervous system (CNS), as it may bypass first-pass metabolism and enable direct or preferential transport to the brain via the olfactory region [16–19]. This approach has the potential to enhance brain targeting while reducing systemic exposure and the high doses required for oral administration.

In this context, the simultaneous delivery of multiple neuroprotective agents may provide additive or synergistic effects, as described in combination therapy approaches [20]. While co-encapsulation strategies in nanosystems such as solid lipid nanoparticles (SLNs) and nanostructured lipid carriers (NLCs) have been proposed to improve the bioavailability of poorly water-soluble drugs [20], they may present limitations related to differential drug partitioning within the lipid matrix and distinct release kinetics of the individual components.

An alternative strategy involves the design of prodrugs capable of incorporating two active moieties within a single molecular entity, enabling their co-delivery at a fixed molar ratio while potentially improving physicochemical properties relevant for encapsulation. In particular, the relatively low lipophilicity of Fer (log P ~1.4) limits its efficient incorporation into lipid-based carriers, as previously demonstrated [21]. This physicochemical limitation represents a key drawback for its direct encapsulation and supports the rationale for a prodrug-based strategy. Indeed, we have previously shown that methylation of Fer to yield its methyl ester (Fer-Me) significantly enhances its encapsulation efficiency in lipid-based carriers [21], and that further optimization can be achieved through dimeric conjugates (Fer-Fer-Me) [11].

Based on these considerations, we designed and synthesized a novel lipophilic prodrug, UDC-Fer-Me (Fig. 1), obtained by ester conjugation of methyl ferulate (Fer-Me) with UDCA. This design combines the mitochondrial-protective properties of UDCA with the antioxidant activity of Fer derivatives, while increasing overall hydrophobicity to facilitate encapsulation into SLNs intended for intranasal delivery. According to the proposed structure, UDC-Fer-Me may undergo enzymatic hydrolysis *in vivo*, leading to the release of UDCA and Fer-Me, the latter retaining antioxidant activity [11]. Therefore, this conjugate can be considered a potential mutual prodrug, although the extent and kinetics of its bioconversion may influence the effective release of the active moieties under physiological conditions.

On this basis, we hypothesized that delivery of UDC-Fer-Me to the brain, followed by its hydrolysis, could provide neuroprotective effects through the combined action of its components. Therefore, the aim of this study was to design, synthesize, and evaluate UDC-Fer-Me as a prodrug suitable for encapsulation into SLNs and for intranasal delivery to the CNS. In particular, we investigated its hydrolysis profile, antioxidant activity in neuronal cells, permeability across nasal epithelial cells, and *in vivo* brain delivery following intranasal administration.

2. Materials and methods

2.1. Materials

Ferulic acid (Fer), carbazole, glacial acetic acid, dimethyl sulfoxide (DMSO), Trizma base (Tris), hydrochloric acid (HCl), sodium taurocholate, chloroform, Dulbecco's Phosphate-Buffered saline (DPBS), 3-(4,5-dimethylthiazol-2-yl)-2,5-diphenyltetrazolium (MTT), N-(4-hydroxyphenyl)retinamide (4-HPR), Neutral red (3-amino-7-dimethylamino-2-methyl-phenazine hydrochloride) (cat. no. N4638), ascorbic acid, 2′,7′-dichlorofluorescin diacetate (DCFH-DA), bovine serum albumin (BSA), and hydrogen peroxide (H_2O_2) were purchased from Merck Life Sciences Srl (Milan, Italy). (High Performance Liquid Chromatography (HPLC)-grade methanol (MeOH) and ethanol (EtOH) were obtained from Carlo Erba Reagents S.A.S. (Milan, Italy). Purified water (H_2O) for HPLC analysis was produced with a Sartorius Arium® Advance EDI system (Sartorius Lab Instruments GmbH & Co., KG, Göttingen, Germany). Methyl ferulate (Fer-Me) was synthesized as previously reported [21]. 1-(3-Dimethylaminopropyl)-3-ethylcarbodiimide hydrochloride (EDCI) was purchased from Carbosynth (Compton, Berkshire, UK), and 4-(dimethylamino)pyridine (DMAP) from Merck (Milan, Italy). Ursodeoxycholic acid (UDCA) was kindly provided by ICE SpA (Reggio Emilia, Italy). Anhydrous N,N-dimethylformamide (DMF) was purchased from Merck (Milan, Italy) and used without further purification.

Dulbecco's modified Eagle's medium (DMEM) with Glutamax, phenol-red-free DMEM, Advanced Minimum Essential Medium (A-MEM), fetal bovine serum (FBS), penicillin, streptomycin, L-glutamine, and trypsin-EDTA were supplied by Thermo Fisher Scientific (Milan, Italy) and Microtech (Naples, Italy). Cell culture vessels and additional reagents were obtained from Thermo Fisher Scientific (Milan, Italy) and Biosigma (Venice, Italy). Compritol 888 ATO, Tween 80, and Span 45 were obtained from Gattefossè Italia (Milan, Italy). Male Wistar rats (200–250 g) were provided by Charles River Laboratories (Calco, Italy). Unless otherwise stated, all reagents and solvents were of analytical grade (Merck Life Sciences Srl, Milan, Italy). FL-70 concentrate was purchased from Fisher Scientific.

2.2. Synthesis of the UDC-Fer-Me conjugate

The synthesis of UDC-Fer-Me (scheme in Fig. 2) was performed via Steglich-like esterification reaction and was monitored by TLC on precoated silica gel F_{254} plates (thickness, 0.25 mm; Merck, Italy), developed with phosphomolybdic acid solution. Flash column chromatography was performed on silica gel (60 Å, 230–400 mesh,

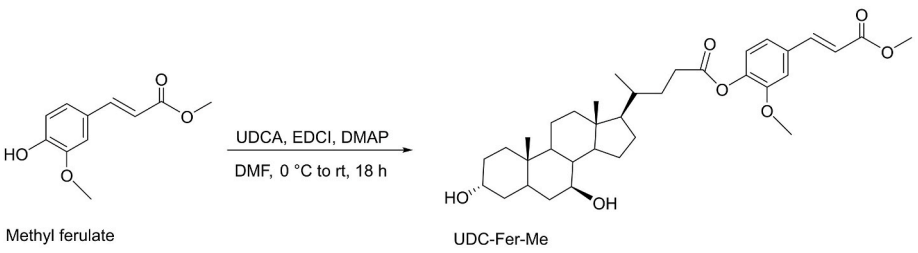

Fig. 2. Synthesis of UDC-Fer-Me via Steglich-type esterification reaction.

Merck, Italy). NMR spectra were recorded with a Varian Mercury 400 MHz instrument in DMSO-d_6. ESI-MS were acquired on an ESI MICROMASS ZMD 2000.

A solution of UDCA (0.94 g, 2.39 mmol) and methyl ferulate [21] (0.55 g, 2.63 mmol) in anhydrous DMF (5 mL) was cooled (ice bath) under an Argon atmosphere, then DMAP (0.35 g, 2.87 mmol) and EDCI (0.55 g, 2.87 mmol) were added. After 10 min at 0 °C, the reaction was warmed up to room temperature and stirred for 18 h, then treated with an ice-cold solution of 5% HCl (10 mL) to form a white precipitate. The precipitate was filtered out using a Büchner funnel and washed with ice-cold distilled water (10 mL), then dried. The crude powder was purified by flash chromatography (EtOAc/Cy 3:1) to give 1.08 g of pure UDC-Fer-Me.

2.2.1. Calculated Log $P_{o/w}$ values of UDCA, Fer, Fer-Me, and UDC-Fer-Me

The logarithmic octanol-water partition coefficient (Log $P_{o/w}$) of UDCA, Fer, Fer-Me and the ester conjugate UDC-Fer-Me were calculated using both the SwissADME system [22] and the ChemDraw Ultra software, version 12.0.2.1076 (PerkinElmer PerkinElmer Informatics, Waltham, MA, USA).

2.3. Solubility of the UDC-Fer-Me conjugate and stock solutions

Solubility of UDC-Fer-Me was determined in water, in 10 mM acetate buffer (pH 5.5) supplemented with 0.1% BSA and 0.05% sodium taurocholate, and in a H_2O/MeOH (50:50, v/v) mixture. An excess of UDC-Fer-Me (5 mg/mL) was added to 3 mL of solvent and equilibrated for 36 h at room temperature in the dark and under stirring. After filtration and dilution, samples (10 μL) were injected into the HPLC (section 2.7) for quantification.

Stock solutions (10^{-2} M) of UDC-Fer-Me, Fer-Me, Fer, and carbazole (internal standard) were prepared in DMSO and stored at −20 °C until use.

2.4. Preparation of rat liver and brain homogenates

Male Wistar rats were sacrificed by decapitation after light isoflurane anesthesia. Liver and brain tissues were rapidly isolated on ice, washed, and homogenized (liver in 4 vol, brain in 5 vol of Tris-HCl buffer 50 mM, pH 7.4, 4 °C). Liver homogenates were prepared with a Potter-Elvehjem homogenizer; brain homogenates with an Ultra-Turrax (3 × 15 s bursts). After centrifugation (liver: 2000×*g*, 10 min, 4 °C; brain: 3000×*g*, 15 min, 4 °C), supernatants were stored at −80 °C. Protein concentration was determined by the Lowry method [23], resulting in 28.3 ± 1.0 μg/μL for liver and 8.0 ± 0.3 μg/μL for brain homogenates.

2.5. Kinetic analysis in Tris-HCl

Kinetic analysis of UDC-Fer-Me was performed by its incubation at 37 °C in a mixture of Tris-HCl buffer 50 mM (pH 7.4) and MeOH 70:30 (v/v) at a final concentration of 30 μM (17.5 μg/mL), obtained by dilution of the stock solution. The dissolution experiments in water described in section 2.3 did not yield detectable amounts of solubilized UDC-Fer-Me by HPLC, indicating that this compound is practically insoluble in water. Consequently, MeOH was necessary for the dissolution of this compound in the incubation medium for kinetic analysis in Tris-HCl. At defined time points, the samples (150 μL) were withdrawn and, after filtration (regenerated cellulose, 0.45 μm), 10 μL was injected into the HPLC apparatus (section 2.7) for the quantification of UDC-Fer-Me and its potential hydrolysis products. Three independent incubation experiments were performed, and the results were presented as the mean of the values.

2.6. Kinetic analysis in rat liver and rat brain homogenate

UDC-Fer-Me (30 μM, 17.5 μg/mL) was incubated in 3 mL of rat liver or brain homogenates at 37 °C. At defined time intervals, 100 μL homogenate aliquots were withdrawn, mixed with 250 μL EtOH and 50 μL carbazole (100 μM in EtOH), centrifuged (13,500×*g*, 10 min), dried under a nitrogen stream (300 μL), and resuspended in 150 μL H_2O/MeOH (50:50, v/v). After double centrifugation (16,000×*g*, 5 min), 15 μL was analyzed by HPLC. Results are the means of three independent experiments.

2.7. HPLC analysis

The quantification of UDC-Fer-Me and its potential hydrolysis products Fer-Me and Fer was conducted by using a modular HPLC system, which comprised a pump (model LC-40D), a DAD detector (model SPD-M40, Shimadzu, Kyoto, Japan), and an injection valve with a 20-μL sample loop (model 7725; Rheodyne, IDEX, Torrance, CA, USA).

The elution was performed by using a 5-μm Hypersil BDS C-18 column (150 mm × 4.6 mm i.d.; Thermo-Fisher Scientific SpA Italia Srl, Milan, Italy) accompanied by a guard column packed with the same Hypersil material. UDC-Fer-Me and its potential hydrolysis products Fer-Me and Fer were separated at room temperature using a mobile phase consisting of a mixture of acidified H_2O (0.4% v/v acetic acid) and MeOH, with a ratio determined by a gradient profile, with a flow rate of 0.8 mL/min. Specifically, an isocratic elution was performed for 3 min using 55% (v/v) of MeOH in the aqueous solvent. Following this, a linear gradient was established over 7 min to achieve 80% (v/v) of MeOH in the aqueous solvent, and this ratio was maintained for 10 min. Subsequently, the mobile phase was adjusted back to the initial volume ratio of 55% (v/v) MeOH in the aqueous solvent with a linear gradient over 5 min, and an additional 5 min ensured the system re-equilibration to the initial conditions. The chromatograms were displayed at two different wavelengths to evaluate the absorbance of all compounds: 280 nm for UDC-Fer-Me and carbazole, the latter used as an internal standard during the extraction of rat whole blood and liver/brain homogenates; 320 nm for the potential hydrolysis products Fer-Me and Fer. The retention times of Fer, Fer-Me, carbazole, and UDC-Fer-Me under the analytical conditions described were 3.0, 4.9, 10.7, and 20.5 min, respectively. LabSolutions Software (version 5.110 in Windows 10, Shimadzu, Kyoto, Japan) was used for data acquisition and processing.

Repeated analyses (n = 6) of the same sample solution containing every single compound at 10 μM concentration (1.94 μg/mL for Fer; 2.08 μg/mL for Fer-Me; 5.83 μg/mL for UDC-Fer-Me) dissolved in

MeOH, or in a mixture of H_2O and MeOH (50:50 v/v), or in a mixture of Tris-HCl buffer 50 mM (pH 7.4) and MeOH (70:30 v/v), and at 3 μM concentration (0.58 μg/mL for Fer; 0.62 μg/mL for Fer-Me; 1.75 μg/mL for UDC-Fer-Me) in 10 mM acetate buffer (pH 5.5) supplemented with 0.1% BSA and 0.05% sodium taurocholate, were used to determine the chromatographic precision, represented by relative standard deviation (RSD) values ranging from 0.87 to 0.95. Calibration curves of peak areas in function of concentration, the latter ranging from 0.1 to 10 μM for each compound in 10 mM acetate buffer (pH 5.5) supplemented with 0.1% BSA and 0.05% sodium taurocholate (0.019–1.94 μg/mL for Fer; 0.021–2.08 μg/mL for Fer-Me; 0.058–5.83 μg/mL for UDC-Fer-Me) or from 0.1 to 50 μM for each compound (0.019–9.81 μg/mL for Fer; 0.021–10.41 μg/mL for Fer-Me; 0.058–29.14 μg/mL for UDC-Fer-Me) dissolved in the other media described above, were generated. These curves exhibited linearity within the considered range ($n = 8$, $r \geq 0.994$, $P < 0.001$).

A preliminary analysis was performed on blank rat liver and brain homogenates, CSF, and blood samples to ascertain that the components of these biological matrices do not interfere with the retention times of UDC-Fer-Me, Fer-Me, Fer, and the internal standard (carbazole). CSF was simulated using standard aliquots of DPBS balanced solution depleted of calcium and magnesium and supplemented with 0.45 mg/mL BSA [24,25]. Calibration curves of peak areas *versus* concentration ranging from 0.1 to 10 μM for Fer (0.019 to 1.94 μg/mL), Fer-Me (0.021 to 2.08 μg/mL), and UDC-Fer-Me (0.058 to 5.83 μg/mL), were obtained dissolving the compounds in CSF simulation fluid and exhibited linearity within the considered range ($n = 8$, $r \geq 0.995$, $P < 0.001$). The peak areas obtained from the extraction of blood or liver/brain homogenate test samples (10 μM) at 4 °C ($n = 6$) were compared to those obtained by the injection of solutions of the analytes dissolved in a mixture of H_2O and MeOH (50:50 v/v) at the same concentration; the average recoveries of Fer, Fer-Me, and UDC-Fer-Me extracted resulted approximately in the range from 40% to 89%. The concentrations of these compounds in whole blood or liver/brain homogenates were therefore expressed as peak area ratios with respect to the internal standard, carbazole. The calibration curves in these biological systems at 4 °C, ranging from 0.5 to 50 μM for Fer (0.097 to 9.71 μg/mL), Fer-Me (0.104 to 10.41 μg/mL), and UDC-Fer-Me (0.291 to 29.14 μg/mL, resulted linear ($n = 8$, $r \geq 0.993$, $P < 0.001$).

2.8. Antioxidant activity of UDC-Fer-Me on neuronal differentiated Neu-2A cells

2.8.1. Neu-2A cell culture and neuronal differentiation

The mouse-derived neuroblastoma Neu-2A cell line was seeded in T75 flasks and grown in Dulbecco's Modified Eagle Medium (DMEM) containing Glutamax, supplemented with 100 μg/mL streptomycin, 100 IU/mL penicillin, and 10% fetal bovine serum (FBS) in a humidified 5% CO_2 atmosphere at 37 °C. After two passages by trypsinization, the cells were seeded at a density of 5×10^3 cells/well in 96-well plates with 0.2 mL of growth DMEM medium. A Scepter™ 2.0 handheld automated cell counter (Merck Millipore, Milan, Italy) was used for cell counting. Neuronal differentiation protocol was adapted from previously reported methods with minor modifications [26,27]; cells were allowed to adhere for 24 h; the growth medium was then replaced with a differentiating medium composed of DMEM containing Glutamax, 1% FBS, and 1 μM N-(4-hydroxyphenyl)retinamide (4-HPR). Differentiation was continued for up to 8 days, after which the cells were used for experiments.

2.8.2. MTT assay for evaluation of UDC-Fer-Me toxicity on differentiated neuronal cells

The potential neurotoxicity of UDC-Fer-Me in differentiated Neu-2A cells, seeded at a density of 5×10^3 cells/well and neuronally differentiated as described above, was assessed using the MTT assay. Cells were incubated for 1 h at 37 °C in a humidified 5% CO_2 atmosphere with increasing concentrations (1, 5, 10, 40, 70, and 100 μM) of UDC-Fer-Me or with 100 μM ascorbic acid (used as a known antioxidant positive control), both dissolved in 0.2 mL of differentiating DMEM medium without 4-HPR. After incubation, the sample media were removed, and 0.2 mL of MTT solution (0.5 mg/mL) in differentiating DMEM medium without 4-HPR was added to each well (4 h; 37 °C; 5% CO_2). Metabolically active cells reduced the insoluble yellow tetrazolium salt into purple formazan crystals. After incubation, the MTT solution was discarded and the formazan crystals were solubilized for 1 h (37 °C) in DMSO (0.1 mL/well) while shaking in an orbital incubator (VDRL Stirrer with Thermostatic Cupola, Model 711/CT +, Asal Srl, Cernusco, Milan, Italy). The absorbance of each well was measured at 570 nm using a microplate reader (NB-12-0035 Microplate Reader, NeoBiotech, distributed by CliniSciences, Rome, Italy), using blank and cell-free wells with test concentrations of UDC-Fer-Me as reference. Cell viability was expressed as the percentage of MTT reduction in treated cells relative to untreated controls (set as 100% viability). Each reported value represents the mean of three independent experiments, each performed in duplicate ($n = 6$).

2.8.3. Neutral red uptake assay for the assessment of UDC-Fer-Me toxicity in neuronally differentiated Neu-2A cells

The potential neurotoxicity of UDC-Fer-Me in differentiated Neu-2A cells was also tested by Neutral Red (NR) cytotoxicity test, following the method reported by Repetto et al. [28]. Briefly, cells were seeded at a density of 5×10^3 cells/well in 96-well plates, neuronally differentiated as described above and then incubated for 1 h at 37 °C in a humidified 5% CO_2 atmosphere with increasing concentrations (1, 5, 10, 40, 70, and 100 μM) of UDC-Fer-Me. UDC-Fer-Me in the same range of concentrations was also incubated in parallel cell-free wells at the same conditions to dismiss possible chemical interaction of increasing concentrations of UDC-Fer-Me with NR dye. At the end of incubation, each well was rinsed once with 200 μL of DPBS Ca^{2+} and Mg^{2+} free, a NR solution in DPBS (3 mg/mL) was diluted 1:100 in culture medium containing 1% FBS and 150 μL of 30 μg/mL NR were added to each well. After a 3 h of incubation at 37 °C, NR solution was removed, each well was rinsed once with 200 μL of DPBS and dye extraction was performed by adding 150 μL of NR destain acidified ethanol solution (50% ethanol 96%, 49% deionized water, 1% glacial acetic acid) into each well. The 96-well plate was gently shaken for 10 min at RT, and the OD of NR extract was measured at 540 nm in a microtiter plate reader spectrophotometer (NB-12-0035 Microplate Reader, NeoBiotech, distributed by CliniSciences, Rome, Italy), using blank and cell-free wells with test concentrations of UDC-Fer-Me as reference. Cell viability was expressed as the percentage of NR extraction in treated cells relative to untreated controls (set as 100% viability). Each reported value represents the mean of three independent experiments, each performed in duplicate ($n = 6$).

2.8.4. Detection of reactive oxygen species (ROS) in differentiated Neu-2A cells treated with UDC-Fer-Me and stressed with H_2O_2

The potential antioxidant effect of UDC-Fer-Me was evaluated using the method described by Wang and Joseph [29,30]. In this method, the nonpolar probe 2′,7′-dichlorofluorescin diacetate (DCFH-DA) enters intact cells and is hydrolyzed by intracellular esterases to form the nonfluorescent DCFH carboxylate anion. This anion remains trapped within the cells and, upon oxidation by free radicals generated by stressors such as hydrogen peroxide (H_2O_2), is converted into highly fluorescent dichlorofluorescin (DCF). The fluorescence intensity of DCF thus reflects the intracellular ROS production.

Neu-2A cells were seeded at a density of 5×10^3 cells/well in OptiPlate® 96-well plates (black-coated, clear bottom) and neuronally differentiated as described above. After 8 days, the differentiating medium was replaced with pre-warmed phenol-red-free and serum-free DMEM supplemented with 10 μM DCFH-DA. Cells were incubated for 30 min in the dark in a humidified 5% CO_2 atmosphere at 37 °C. The DCFH-DA loading solution was then removed, and the cells were washed

twice with fresh phenol-red-free and serum-free DMEM to remove extracellular, non-internalized probe. Subsequently, Neu-2A cells were pre-incubated for 1 h in a humidified 5% CO_2 atmosphere at 37 °C with one of the following: (*i*) phenol-red-free DMEM containing 1% FBS (untreated control), (*ii*) UDC-Fer-Me (1, 5, or 10 μM), or (*iii*) 100 μM ascorbic acid (antioxidant positive control), all dissolved in phenol-red-free DMEM containing 1% FBS.

After this pre-treatment, H_2O_2 was added (final concentration 100 μM) in the absence or presence of UDC-Fer-Me or ascorbic acid. Fluorescence intensity, reflecting the oxidation of DCFH to DCF by intracellular ROS generated in response to H_2O_2, was measured at an excitation wavelength of 485 nm and an emission wavelength of 530 nm, with readings taken over a 60-min time course using a fluorescence microplate reader (EnSight™ Multimode Plate Reader, PerkinElmer, Milan, Italy) maintained at 37 °C. Results are expressed as the percentage of intracellular ROS production relative to untreated controls (100%), and represent the mean ± S.E.M. from sextuplicate wells (n = 6).

2.9. Uptake studies in respiratory mucosa RPMI 2650 cells

2.9.1. RPMI 2650 cell culture

RPMI 2650 cells were used to investigate *in vitro* the potential cell uptake of UDC-Fer-Me as free compound incubated at non-cytotoxic concentrations. This cell line derives from an anaplastic squamous cell carcinoma of the human nasal septum and displays epithelial morphology [31,32], making it a suitable *in vitro* model for respiratory mucosa.

RPMI 2650 cells were cultured in 75 cm^2 polystyrene flasks with Advanced Minimum Essential Medium (A-MEM) containing 2 mM L-glutamine, 100 μg/mL streptomycin, 100 IU/mL penicillin, and 10% FBS at 37 °C in a 5% CO_2 atmosphere. Cells were split twice with trypsin-EDTA at 37 °C before being seeded and allowed to grow to approximately 90% confluence for MTT assays and uptake studies. A Scepter™ 2.0 handheld automated cell counter (Merck Millipore, Milan, Italy) was used for cell counting.

2.9.2. MTT assay for evaluation of UDC-Fer-Me toxicity on RPMI 2650 cells

RPMI 2650 cells were seeded in a 96-well plate at a density of 3×10^4 cells/well in 0.2 mL of growth A-MEM. The potential cytotoxicity of UDC-Fer-Me as a free compound was assessed using the MTT assay. To this end, cells were incubated for 1 h under standard conditions (37 °C and 5% CO_2) with increasing concentrations of UDC-Fer-Me (1, 5, 10, 40, 70, and 100 μM) dissolved in growth A-MEM. After the incubation period, the sample media were discarded, and 0.2 mL of MTT solution (0.5 mg/mL) in growth A-MEM was added to each well and incubated (3 h; 37 °C; 5% CO_2). After incubation, the MTT solution was discarded, and the resulting formazan crystals were solubilized for 1 h (37 °C) in DMSO (0.1 mL/well) while shaking in an orbital incubator. The absorbance of each well was measured at 570 nm using a microplate reader (NB-12-0035 Microplate Reader, NeoBiotech, distributed by CliniSciences, Rome, Italy). Cell viability was expressed as the percentage of MTT reduction in cells treated with culture medium (untreated control set at 100% viability) compared to those treated with UDC-Fer-Me. Each reported value represents the mean of three independent incubation experiments, each performed in duplicate (n = 6).

2.9.3. Time-course of UDC-Fer-Me uptake in respiratory nasal mucosa RPMI 2650 cells

RPMI 2650 cells were seeded in a 12-well plate at a density of 8×10^4 cells/well in 2 mL of culture A-MEM medium. After 24 h of culture, the potential uptake of UDC-Fer-Me by RPMI 2650 cells as a free compound was evaluated by adding a solution of UDC-Fer-Me (100 μM) in complete A-MEM medium to the test wells and incubating the plate for predetermined time intervals (10, 30, and 60 min) in a humidified 5% CO_2 atmosphere at 37 °C. At the end of each incubation period, the sample media were removed. The adherent cells were then rinsed three times with DPBS supplemented with 0.9 mM $CaCl_2$, 0.5 mM $MgCl_2$, and 5 mM glucose (2 mL), followed by lysis with 0.2 mL of chilled bi-distilled water (approximately 4 °C) and storage at −80 °C for at least 30 min. After thawing, 0.2 mL of MeOH was added to the wells to ensure complete solubilization of UDC-Fer-Me. The lysate was centrifuged twice (13,500×*g* for 10 min), and the supernatant was immediately injected into the HPLC system (20 μL) for the quantification of UDC-Fer-Me and its potential hydrolysis products Fer-Me and Fer (see section 2.7). In parallel, cell-free wells were incubated under the same conditions (time points and UDC-Fer-Me concentrations) in culture medium and processed as described for cell-containing wells, including washing, freezing, and methanol addition, in order to assess potential extracellular precipitation or sedimentation of the prodrug. Normalization of UDC-Fer-Me uptake to cell number was performed by detaching cells with trypsin in untreated wells at the end of the experiments, counting them using the Scepter™ 2.0 automated cell counter (Merck Millipore, Milan, Italy). Each reported value represents the mean of three independent incubation experiments and is expressed as nanomoles of compound per 10^6 cells.

2.10. Preparation of UDC-Fer-Me conjugate-loaded nanoparticles

Solid lipid nanoparticles (SLNs) were prepared using the emulsification/evaporation solvent technique. First, the organic phase was prepared by dissolving Compritol ATO 888 (120 mg), Span 85 (40 mg), and UDC-Fer-Me (30 mg) in 3 mL of chloroform. This phase was then added dropwise into 5 mL of an aqueous phase containing Tween 80 (1% w/v) and sodium taurocholate (1% w/v), while homogenizing the mixture with an Ultra-Turrax T25 (IKA-Werk, Staufen, Germany) at 24,000 rpm for 5 min. The resulting oil-in-water emulsion was immediately poured into 15 mL of water placed in an ice bath and sonicated at 20 W for 3 min (Ultrasonic Cell Disruptor Microson, Model XL 2005, Farmingdale, NY). The organic solvent was then evaporated while maintaining the suspension under magnetic stirring for 2 h at room temperature. Finally, the SLNs were purified by dialysis for 30 min (molecular weight cut-off 12,000–14,000 Da; Merck Life Sciences Srl, Milan, Italy) and freeze-dried for 24 h to obtain dry, water-free nanoparticles (FreeZone 2.5, Labconco Corporation, Kansas City, Missouri, USA). Unloaded nanoparticles were prepared following the same procedure, omitting the addition of UDC-Fer-Me.

2.11. Characterization of UDC-Fer-Me conjugate-loaded nanoparticles

The unloaded and UDC-Fer-Me-loaded SLNs were characterized as follows: (*i*) by scanning electron microscopy (SEM) to assess particle morphology; (*ii*) by centrifugal field-flow fractionation (CFFF) and dynamic light scattering (DLS, also known as photon correlation spectroscopy, PCS) to analyze particle size distribution; (*iii*) by high-performance liquid chromatography (HPLC) to determine drug loading (DL%) and encapsulation efficiency (EE%); and (*iv*) by differential scanning calorimetry (DSC) to investigate possible interactions between the lipid matrix and the encapsulated compound.

2.11.1. Morphological evaluation of the SLNs

A scanning electron microscope (SEM) equipped with a Field Emission Gun (FEG) emitter (Zeiss Gemini 460, Carl Zeiss GmbH, Germany) was used to observe the morphology of the nanoparticles. An aqueous SLN suspension was dropped and left to dry on a glass support, which was, afterwards, attached to a carbon tape on the proper stub. After gold sputtering (Q150R, Quorum Technologies, United Kingdom), imaging parameters were:

- high vacuum mode;
- InLens detector and secondary electrons (SE);

– 5 kV as acceleration voltage.

2.11.2. Size distribution analysis of the SLNs

SLNs size distribution was determined by either Dynamic Light Scattering (DLS or PCS) and CFFF.

Dynamic Light Scattering measurements were done by using a Zetasizer Pro (Malvern Instr., Malvern, England) with a 5 mW helium neon laser and a wavelength output of 633 nm. Measurements at a 173° angle were performed at 25 °C and with a run time of 120 s. Samples were diluted with deionized water (Milli-Q) in a 1:10 v/v ratio and analyzed in triplicate.

For the zeta potential (ζ) measurements, each SLN dispersion was diluted 10-fold in deionized water; the prepared samples were transferred by syringe into a U-shaped capillary cell (DTS1070). The ζ value was measured three times during one cycle and was then calculated by the system software using the Smoluchowski equation. The arithmetic mean and standard deviation of the results were calculated over five repeated measurements.

The CFFF system was described elsewhere (Model S101, Postnova Analytics GmbH, Germany FFFractionation, Inc., Salt Lake City, UT, USA) [33]. The mobile phase was constituted of a 0.1% v/v solution of FL70 in deionized Milli-Q water (Millipore S.p.A., Vimodrone, Milan, Italy) pumped at 1.0 mL/min. Fifty microliter samples were directly injected through a 50 μL Rheodyne loop valve. The centrifugal field was programmed according to the following parameters: initial field $G_0 = 2000$ rpm, relaxation time = 5 min, $t_1 = 10$ min, $t_a = -40$ min, $p = 8$, and final field $G_0 = 20$ rpm. The SLNs particle density was assumed $\rho_p = 1.06$ g/mL.

2.11.3. UDC-Fer-Me content in SLNs

Approximately 5 mg of nanoparticles were accurately weighed using a high-precision analytical balance (d = 0.01 mg; Sartorius, model CP 225D, Goettingen, Germany) and subsequently dissolved in MeOH by heating at 80 °C for 5 min. After cooling to room temperature, the solution volume was adjusted to 2 mL with MeOH, then filtered through a regenerated cellulose membrane (0.45 μm) and further diluted 1:10 with fresh MeOH. UDC-Fer-Me was quantified by injecting 10 μL of the diluted solution into the HPLC system.

The drug loading (DL %) and drug entrapment efficiency (EE %) were calculated according to the following equations (1) and (2):

$$\text{DL \%} = \frac{\text{Amount of incorporated prodrug}}{\text{Total mass of dried sample}} \times 100 \quad (1)$$

$$\text{EE \%} = \frac{\text{Amount of drug in purified sample}}{\text{Total amount of prodrug used}} \times 100 \quad (2)$$

Results derive from three independent experiments and are presented as mean ± S.E.M.

2.11.4. Differential scanning calorimetry

Differential scanning calorimetry (DSC) analysis was carried out with a PerkinElmer (DSC 7, Shelton, CT, United States). The samples had a typical mass of 2–4 mg, measured using a high precision analytical balance (d = 0.01 mg; Sartorius, model CP 225D, Goettingen, Germany). They were put in non-hermetic aluminum pans, and an empty aluminum pan was used as a reference. The measurements were performed in the 40–250 °C temperature interval, at a heating rate of 2 °C/min, under a continuous purged dry nitrogen flux (20 mL/min). Indium and zinc standards were used for instrument calibration, in order to cover the whole range of temperatures investigated. The data were collected in triplicate for each sample.

2.12. Stability analysis of UDC-Fer-Me in H_2O:MeOH mixture and acetate buffer (pH 5.5)

The stability of 10 μM UDC-Fer-Me was evaluated in H_2O/MeOH solvent mixture (50:50 v/v, 30 mL) maintained under mechanical stirring (100 rpm) at 37 °C for about 8 h. Similarly, UDC-Fer-Me stability at 3 μM concentration was evaluated in 10 mM acetate buffer (pH 5.5) supplemented with 0.1% BSA and 0.05% sodium taurocholate. During the incubation, 150 μL samples were withdrawn and filtered (regenerated cellulose, 0.45 μm), then 10 μL of the filtered solutions was immediately injected into the HPLC apparatus to quantify UDC-Fer-Me and its potential hydrolysis products Fer-Me and Fer. All the values were obtained as the mean of three independent experiments.

2.13. UDC-Fer-Me in vitro dissolution and release studies from SLNs

UDC-Fer-Me or UDC-Fer-Me-loaded SLNs were accurately weighed using an analytical balance (Sartorius CP 225D) and suspended in 100 mL of two different media: (*i*) a H_2O/MeOH mixture (50:50, v/v) to obtain a final UDC-Fer-Me concentration of 20 μM (11.6 μg/mL), corresponding to approximately 10% of the compound's saturation solubility, and (*ii*) a 10 mM acetate buffer (pH 5.5) supplemented with 0.1% BSA and 0.05% sodium taurocholate to obtain a final concentration of 6 μM (3.50 μg/mL), corresponding to approximately 30% of the compound's saturation solubility in this system.

The suspensions were incubated at 37 °C under mechanical stirring (100 rpm), and 150 μL aliquots were withdrawn at predefined time points. Samples from the raw UDC-Fer-Me suspension were filtered through regenerated cellulose filters (0.45 μm), whereas aliquots from the SLN suspensions were filtered upon centrifugation at 13,000×*g* by using Microcon filter devices (YM 30, Millipore Corporation, Bedford, MA, USA; the filters are able to retain nanoparticles larger than the cutoff corresponding to proteins with molecular weight of 30 kD, which is estimated to be approximately 5 nm [34]). In both cases, 20 μL of each filtered sample was injected into the HPLC system for UDC-Fer-Me quantification. All reported values represent the mean of three independent experiments.

2.14. Intravenous infusion to rats of UDC-Fer-Me and kinetic analysis

Male Wistar rats (200–250 g; n ≥ 4) were anesthetized and infused intravenously (femoral vein) with 500 μg UDC-Fer-Me (2 mg/kg) at 0.2 mL/min for 5 min (0.5 mg/mL of UDC-Fer-Me in 80% saline with 0.82 mg/mL sodium taurocholate, 10% EtOH, 10% DMSO). At the administered dose, no evident acute adverse effects were observed in treated animals. This vehicle was employed exclusively for comparative pharmacokinetic purposes and does not represent a clinically translatable formulation. Blood (100 μL) and CSF (30 μL) samples were collected at fixed time intervals. Blood samples were serially collected from the tail vein using a butterfly needle to minimize animal stress and allow repeated sampling. Immediately after sample collection, blood samples were hemolyzed with 500 μL of ice-cold water; 50 μL of 10% sulfosalicylic acid and 50 μL of internal standard (100 μM carbazole dissolved in a water-methanol mixture 50:50 v/v) were then added. The samples were extracted twice with 900 μL of ethyl acetate and, after centrifugation (12,000×*g* for 10 min), the organic layer was reduced to dryness at room temperature under a nitrogen stream. Then, 150 μL of a water-methanol mixture (50:50 v/v) was added to the dried samples and, after double centrifugation, 10 μL was injected into the HPLC system (section 2.7) for Fer, Fer-Me, and UDC-Fer-Me quantification.

CSF samples were collected by the cisternal puncture method described by van den Berg et al. [35], requiring a single needle stick and allowing the collection of serials (about 30 μL) virtually blood-free CSF samples [36]. A maximum of about 120 μL of CSF was collected as total volume from each rat, allowing the restoration of the CSF physiological volume by choosing appropriate time points (n = 4-6, taking into account a maximum of three collections for each rat). The CSF samples (10 μL) were immediately injected into the HPLC system (section 2.7) for Fer, Fer-Me, and UDC-Fer-Me detection. All the values were obtained as the mean of at least four independent experiments.

2.15. Nasal administration of UDC-Fer-Me

UDC-Fer-Me was nasally administered at a dose of approximately 2 mg/kg (0.5 mg per rat) either as the free compound (water suspension) or encapsulated in compritol SLNs. Each nasal formulation was administered to a group of at least four anesthetized adult male Wistar rats (200–250 g body weight), fasted for 24 h, and positioned on their backs. Each rat received, in each nostril, 55 μL of a water suspension containing 5 mg/mL raw UDC-Fer-Me, or an equivalent amount of loaded SLNs corresponding to 5 mg/mL UDC-Fer-Me (62.9 mg/mL of loaded SLNs). A semiautomatic pipette equipped with a short polyethylene tube, inserted approximately 0.6–0.7 cm into each nostril, was used for nasal administration. Blood samples (100 μL) and CSF samples (approximately 30 μL) were collected serially at fixed time points after administration and processed as described in section 2.14 for the quantification of Fer, Fer-Me, and UDC-Fer-Me. All reported values represent the mean of at least four independent experiments.

The trapezoidal method was used to calculate the area under the concentration-time curves (AUC, μg mL^{-1}•min) in the rat bloodstream or CSF following nasal administration of UDC-Fer-Me. The absolute bioavailability (F) of nasally administered UDC-Fer-Me was calculated as the ratio between the nasal AUC and the intravenous (IV) AUC of UDC-Fer-Me measured in the bloodstream, normalized with respect to the administered doses, according to the following Equation (3) [37]:

$$F = \frac{AUC_{nasal}}{AUC_{IV}} \cdot \frac{dose_{IV}}{dose_{nasal}} \quad (3)$$

The computer program GraphPad Prism version 7.0 (GraphPad Software, San Diego, California, U.S.A.) was used to perform the calculations.

The animal study protocol was approved by the Italian Ministry of Health (Rome, Italy; approval number 173/2024-PR) and all procedures were conducted in accordance with the ARRIVE guidelines and the European Directive 2010/63/EU for animal experiments.

2.16. In vitro and in vivo pharmacokinetic calculations

The UDC-Fer-Me degradation in rat liver and brain homogenates, or its elimination from the bloodstream after intravenous infusion, were analyzed as exponential decay plots of the compound concentrations *versus* incubation time, and the related half-life values were obtained from the linear regression of the corresponding semi-logarithmic plots. The quality of the fits was evaluated by considering the correlation coefficients (r) and P values.

The trapezoidal method was used to calculate the area under concentration curves (AUC, μg mL^{-1}·min) in the rat bloodstream or CSF following the intravenous administration of UDC-Fer-Me.

All the calculations were performed by using the computer program GraphPad Prism version 7 (GraphPad Software, San Diego, CA, USA).

2.17. Statistical analysis

Data from MTT assays (sections 2.8.2 and2.9.2) were analyzed by one-way ANOVA with Dunnett's post hoc test. ROS data (section 2.8.3) were analyzed by two-way ANOVA with Tukey's multiple comparison test. All analyses were performed with GraphPad Prism v8.0 (GraphPad Software, San Diego, CA, USA). A P value < 0.05 was considered statistically significant.

3. Results

3.1. Synthesis and characterization of UDC-Fer-Me conjugate

The synthesis of UDC-Fer-Me was carried out in Steglich esterification conditions [38] by using *N*-(dimethylamino)pyridine (DMAP) and 1-ethyl-3-(3-dimethylaminopropyl)carbodiimide (EDCI) as a coupling reagent; the desired compound was obtained in high yield after purification by flash chromatography (78%). After 18 h at room temperature (25 °C), TLC analysis showed the almost total loss of UDCA (limiting reagent), allowing the workup of the reaction. This only required the separation by filtration of powdered UDC-Fer-Me, resulting after treating the reaction with a few mL of a slightly acidic aqueous solution. It is noteworthy that the coupling reagent EDCI, unlike *N, N′*-dicyclohexylcarbodiimide (DCC), simplifies the purification of the desired ester by forming a water-soluble urea byproduct, which can be removed during workup and does not pose appreciable hazards to human health and the environment [39]. After purification by flash chromatography, UDC-Fer-Me was a white powder and was completely insoluble in water, while in 10 mM acetate buffer (pH 5.5) supplemented with 0.1% BSA and 0.05% sodium taurocholate, and in a 50:50 (v/v) H_2O/MeOH mixture its saturation concentrations were 21.4 μM (12.5 μg/mL) and 191.6 μM (111.7 μg/mL), respectively.

^{1}H NMR (Fig. S1): $\delta = 7.63$ (d, 1H, $J = 16.0$ Hz), 7.49 (s, 1 H), 7.28 (d, 1 H, $J = 8.4$ Hz), 7.08 d, 1 H, $J = 8.4$ Hz), 6.68 (d, 1H, $J = 16.0$ Hz), 4.41 (s, 1 H), 3.85 (d, 1 H, $J = 8.0$ Hz), 3.79 (s, 3 H), 3.71 (s, 3 H), 3.36-3.20 (m, 2 H), 2.62-2.52 (m, 1 H), 2.50-2.40 (m, 1 H), 1.98-0.97 (m, 24 H), 0.92 (d, 3 H, $J = 6.4$ Hz), 0.85 (s, 3 H), 0.62 (s, 3 H).

^{13}C NMR (Fig. S2): δ = 171.79, 167.11, 151.62, 144.40, 141.52, 133.38, 123.60, 121.98, 118.51, 112.47, 70.16, 69.88, 56.46, 56.28, 55.12, 51.91, 43.57, 43.45, 42.61, 39.15, 38.17, 35.27, 35.21, 34.20, 31.11, 30.83, 23.75, 18.67, 12.50.

MS (ESI, ES+): Calcd for $[C_{35}H_{50}O_7 + H]^+$ 583.37; Found 583.58.

3.1.1. Calculated Log $P_{o/w}$ values of Fer, Fer-Me, UDC, and UDC-Fer-Me

The calculated Log $P_{o/w}$ values of the conjugated UDC-Fer-Me and the compounds UDCA and Fer-Me used for conjugation are reported in Table S1, together with the calculated Log $P_{o/w}$ of Fer. The values were obtained using both the SwissADME system [22] and the ChemDraw Ultra software version 12.0.2.1076 (PerkinElmer PerkinElmer Informatics, Waltham, MA, USA). Both the two calculation systems evidence that the methylation of Fer induces an increase of its Log $P_{o/w}$ value of ~0.3 or 0.4 logarithmic unities; moreover, the ester conjugation of UDCA and Fer-Me induces an increase of their Log $P_{o/w}$ value of ~2 and ~4 logarithmic units, respectively, obtaining the conjugate UDC-Fer-Me with a Log $P_{o/w}$ value of ~6.

3.2. Hydrolysis studies of UDC-Fer-Me in rat liver and brain homogenates (in vitro studies)

The potential behavior of UDC-Fer-Me as prodrug was investigated by evaluating its hydrolysis in different physiological media, namely rat liver and brain homogenates, selected to represent the peripheral and central compartments of the body, respectively. The amounts of the prodrug and its potential hydrolysis products (*i.e.,* Fer-Me and Fer) were therefore measured at different time-points during the prodrug incubation in these homogenates.

A Tris-HCl buffer solution (pH 7.4) was used for the preparation of liver and brain homogenates. UDC-Fer-Me remained stable in this buffer for 8 h at 37 °C, indicating that no significant degradation occurred under these conditions. A similar stability was previously reported for Fer-Me and Fer [21]. Therefore, any degradation observed in rat liver or brain homogenates can be attributed to enzymatic processes rather than to the Tris-HCl buffer itself.

In rat liver homogenate, UDC-Fer-Me was degraded with the concomitant appearance of Fer-Me, as shown in Fig. 3A, where all data are reported as the percentage of the overall molar amounts of incubated UDC-Fer-Me. In particular, UDC-Fer-Me was totally degraded within 30 min following a pseudo-first order kinetic, as evidenced by the exponential decay plot reported in Fig. 3A and confirmed by the linearity of the semilogarithmic plot in the inset ($n = 5$, $r = 0.996$; $P < 0.001$), which allowed to calculate the elimination constant (k_{el}) and half-life ($t_{1/2}$) values of 0.238 ± 0.12 min^{-1} and 2.90 ± 0.10 min,

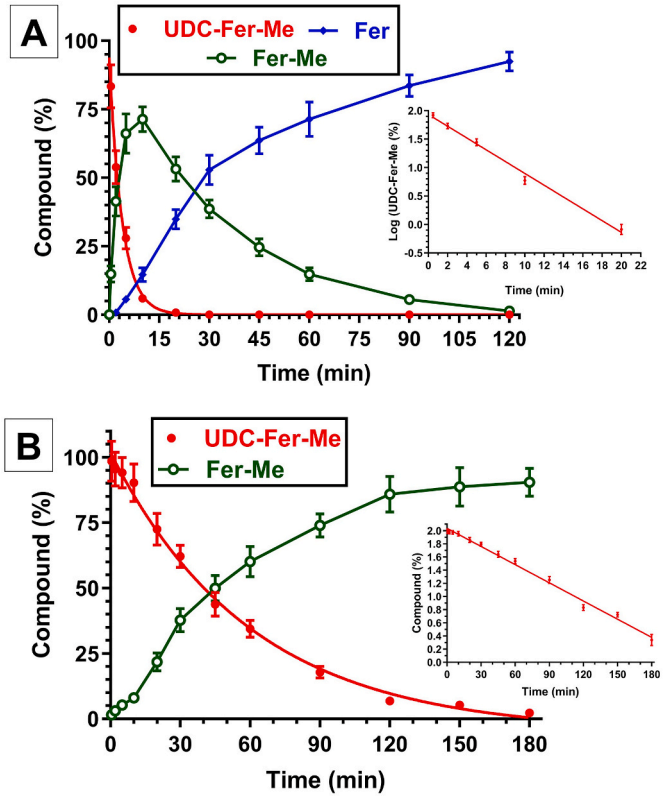

Fig. 3. *In vitro* hydrolysis study in rat liver and brain homogenate. **(A)** Degradation profile of UDC-Fer-Me (red) and the corresponding appearance profiles of Fer-Me (green) and Fer (blue) in rat liver homogenate. The values are reported as the percentage of the overall molar amount of incubated UDC-Fer-Me evidencing the exponential decay of the UDC-Fer-Me amounts, according to a pseudo-first order kinetic, confirmed by the linearity of the semilogarithmic plot reported in the inset (n = 7, r = 0.995, P < 0.001). **(B)** Degradation profile of UDC-Fer-Me (red) and the corresponding appearance profiles of Fer-Me (green) in rat brain homogenate. The values are reported as the percentage of the overall molar amount of incubated UDC-Fer-Me evidencing the exponential decay of the UDC-Fer-Me amounts, according to a pseudo-first order kinetic, confirmed by the linearity of the semilogarithmic plot reported in the inset (n = 11, r = 0.996, P < 0.0001). All data are reported as the mean ± S.E.M. of three independent experiments. (For interpretation of the references to color in this figure legend, the reader is referred to the Web version of this article.)

respectively. The molar amount of Fer-Me released from UDC-Fer-Me increased within the first 15 min to approximately 70% of the total incubated prodrug, then progressively decreased to about 1.5% after 120 min. This decline was accompanied by the formation of Fer, whose molar amount increased over 120 min, reaching approximately 95% of the initial UDC-Fer-Me.

These data indicate that UDC-Fer-Me was degraded by hydrolysis processes (characterized by pseudo-first order kinetics) involving the ester conjugation group between UDCA and Fer-Me; Fer-Me was in turn hydrolyzed to Fer (Fig. 1), at a rate consistent with the previously reported $t_{1/2}$ (about 30 min) in rat liver homogenates [21]. The rat liver homogenate enzymatic activity allows, therefore, to identify UDC-Fer-Me as a prodrug of both Fer and UDCA, at least at the peripheral level. The profiles of UDC-Fer-Me and its degradation products reported in Fig. 3A suggest that hydrolysis of the ester linkage between UDCA and Fer-Me predominates over the hydrolysis of its methyl-ester group, as reported in the scheme of Fig. 1.

In addition to the liver homogenate, the ability of rat brain homogenate to hydrolyze UDC-Fer-Me was evaluated, in order to investigate its potential prodrug behavior in the CNS. The compound was degraded also in rat brain homogenate with the concomitant appearance of Fer-Me, as shown in Fig. 3B, where data are reported as the percentage of the overall molar amounts of incubated UDC-Fer-Me.

In particular, UDC-Fer-Me was progressively degraded, with its amount decreasing to approximately the 2% within 3 h of incubation. The degradation followed a pseudo-first order kinetic, as evidenced by the exponential decay plot reported in Fig. 3B and confirmed by the linearity of the semilogarithmic plot in the inset (n = 11, r = 0.996; P < 0.0001). The data allowed to calculate the k_{el} and $t_{1/2}$ values of 0.021 ± 0.001 min^{-1} and 32.55 ± 0.61 min, respectively.

The Fer-Me molar amounts, released by UDC-Fer-Me degradation, increased over 180 min, reaching approximately 90% of the initially incubated prodrug. In this case, no formation of Fer was detected, consistent with the previously reported inability of rat brain homogenate to hydrolyze Fer-Me [21]. The rat brain homogenate enzymatic activity therefore supports the role of UDC-Fer-Me as a prodrug of both Fer-Me and UDCA in the CNS. The profiles of UDC-Fer-Me and Fer-Me reported in Fig. 3B, together with the absence of detectable Fer amounts in brain homogenates, indicate that, also in this case, the hydrolysis of the prodrug ester conjugation group between UDCA and Fer-Me predominates over the hydrolysis of its methyl-ester group.

3.3. *Antioxidant activity of UDC-Fer-Me on neuronal differentiated Neu-2A cells*

Neuroblastoma Neu-2A cells, a cholinergic cell line capable of differentiating into either cholinergic or dopaminergic neurons depending on culture conditions [40], were used to evaluate the potential of UDC-Fer-Me as an antioxidant agent against H_2O_2-induced oxidative stress in neuronal cells. To ensure accurate evaluation of its potential antioxidant effects, the cytotoxicity of UDC-Fer-Me was first assessed in neuronally differentiated Neu-2A cells using MTT and Neutral Red (NR) uptake assays, in order to exclude confounding concentration-dependent effects on cell viability. In this study, Neu-2A cells were differentiated into neuronal cells, as certain cytotoxic effects are not observed in non-excitable cells such as undifferentiated neuroblastoma cells [41].

3.3.1. *Evaluation of UDC-Fer-Me potential neurotoxicity on neuronal differentiated Neu-2A cells by MTT and neutral red uptake assays*

The viability of Neu-2A cells exposed to increasing concentrations of the compound using a standard MTT assay of the mitochondrial redox activity, was firstly evaluated. As shown in Fig. 4A, treatment with 100 μM ascorbic acid, used as an established antioxidant positive control, did not significantly affect cell viability compared with the untreated control (P > 0.05). Exposure of Neu-2A cells to increasing concentrations of UDC-Fer-Me (1-100 μM) for 1 h, selected to match the time interval of the antioxidant assay, did not adversely affect cell viability. On the contrary, concentrations of 5 μM or higher resulted in a significant increase in cell viability compared with untreated controls (P < 0.0001; Fig. 4A), possibly reflecting enhanced mitochondrial activity. Additionally, cell viability of neuronally differentiated Neu-2A cells exposed to increasing concentrations of UDC-Fer-Me (1-100 μM; 1 h), was evaluated using the NR uptake assay, which relies on the ability of viable cells to incorporate and retain the supravital dye NR within their lysosomes [28]. Compounds that compromise cell membrane or lysosomal integrity reduce NR uptake, resulting in a concentration-dependent decrease in absorbance.

As shown in Fig. 4B, NR uptake confirmed the absence of cytotoxic effects of UDC-Fe-Me at all tested concentrations, in agreement with the MTT assay, despite the different physiological endpoints measured by the two methods. To exclude potential interference from organic solvents, UDC-Fer-Me was directly dissolved in the differentiation medium in both assays.

As illustrated in Fig. 4C, blank wells containing differentiation medium and MTT or NR dye exhibited negligible absorbance, confirming the absence of dye conversion or retention in the absence of cells.

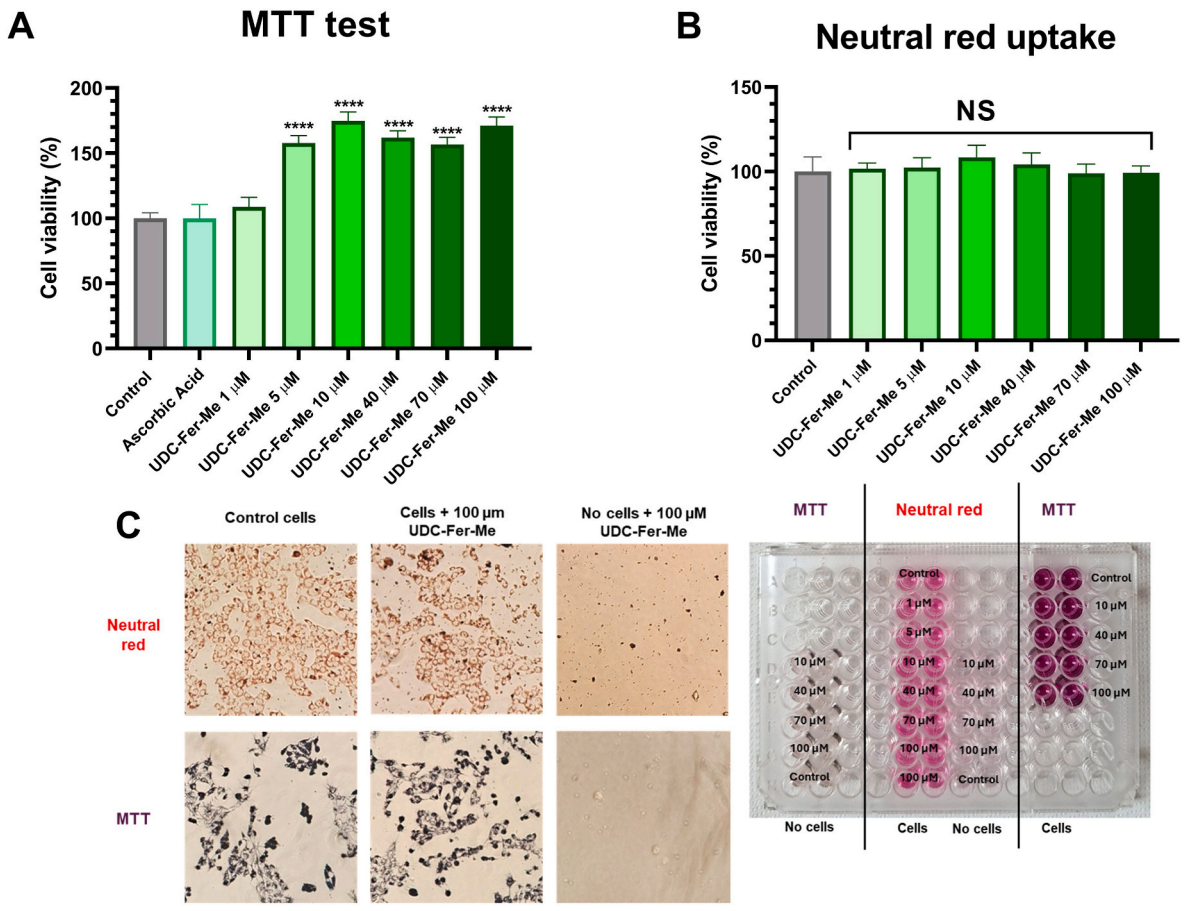

Fig. 4. Effect of different concentrations of UDC-Fer-Me on the viability of neuronally differentiated Neu-2A cells. (**A**) MTT assay. (**B**) Neutral Red (NR) uptake assay. (**C**) Representative results of the MTT and NR assays as phase contrast optical microscope images and in 96-wells plate as well for increasing concentrations of UDC-Fer-Me in the presence and in the absence of cells. ****P < 0.0001: Significant differences compared with the control cells using one-way ANOVA, followed by Dunnett's multiple comparisons test. NS: no significant difference.

Similarly, all tested concentrations of UDC–Fer–Me in cell-free conditions showed minimal absorbance and no visible color change, indicating the lack of direct chemical interaction with either MTT or NR dyes. In contrast, wells containing viable cells showed the expected colorimetric responses (formazan formation in MTT and dye accumulation in NR), with corresponding high absorbance values.

Overall, these results indicate that UDC-Fer-Me does not interfere with the assay readouts and does not induce cytotoxic effects under the

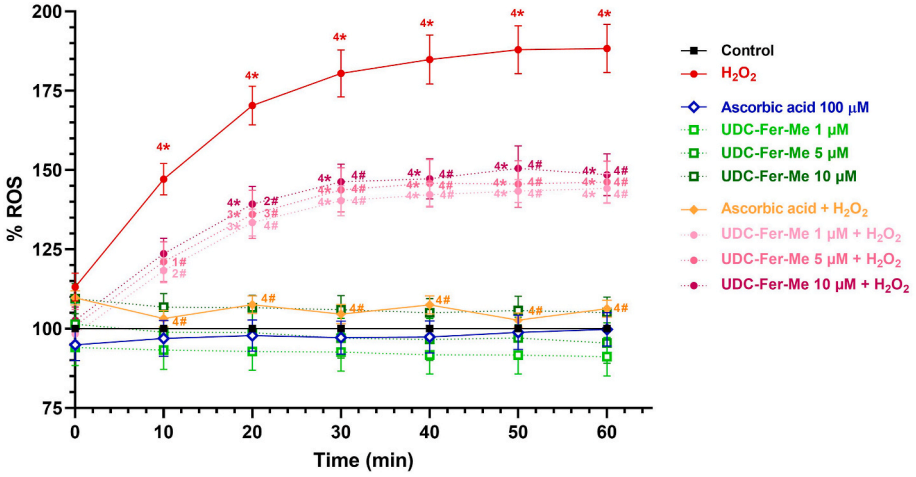

Fig. 5. ROS production in differentiated Neu-2A cells exposed to oxidative stress by H_2O_2 (100 µM) and treatments with UDC-Fer-Me (1, 5, and 10 µM) or ascorbic acid (100 µM). Data are reported as percentages over control cells, and the assay was conducted for 60 min to measure the time-course of intracellular ROS production. Data are expressed as mean ± S.E.M. (n = 6). Statistical comparisons were performed by two-way ANOVA followed by Tukey's multiple comparison test (*: comparison *vs* Control; #: comparison *vs* H_2O_2 -treated cells. The number associated refers to different statistical meanings: 1 = P < 0.05; 2 = P < 0.01; 3 = P < 0.001; 4 = P < 0.0001).

tested conditions, supporting that the observed increase in MTT signal likely reflects enhanced mitochondrial metabolic activity rather than assay artifacts.

3.3.2. UDC-Fer-Me reduces ROS production in neuronal differentiated Neu-2A cells stressed with H_2O_2

Intracellular ROS production was assessed using the DCFH-DA assay (10 μM). As shown in Fig. 5, incubation of Neu-2A cells with UDC-Fer-Me at all tested concentrations (1, 5, and 10 μM) in the absence of H_2O_2 did not significantly increase ROS production compared with the untreated control ($P > 0.05$).

In contrast, exposure to the oxidative stressor H_2O_2 (100 μM) induced a significant, time-dependent increase in DCF fluorescence in Neu-2A cells, indicating enhanced ROS generation compared with the untreated control (set at 100%) at all time points ($P < 0.0001$; Fig. 5). The maximal increase was observed 50 min after H_2O_2 application and remained elevated at the end of the observation period (60 min), reaching a ROS level of 188.31% relative to the untreated control.

Ascorbic acid (a well-established antioxidant compound used as a control) did not alter basal ROS production in neuronal-differentiated Neu-2A cells in the absence of H_2O_2 compared with the untreated control ($P > 0.05$; Fig. 5). However, it completely prevented H_2O_2-induced ROS production ($P < 0.0001$; Fig. 5). In comparison, UDC-Fer-Me partially counteracted the ROS production induced by H_2O_2. When Neu-2A cells were pre-treated for 1 h with increasing concentrations of the prodrug (1–10 μM; 0.58–5.83 μg/mL) prior to H_2O_2 exposure, the resulting ROS levels were significantly lower than those observed in the absence of UDC-Fer-Me (Fig. 5). In particular, at 50 and 60 min after H_2O_2 addition, treatment with 1 μM UDC-Fer-Me reduced ROS production to approximately 144% of the untreated control ($P < 0.0001$), corresponding to roughly a 50% decrease compared with cells exposed to H_2O_2 alone ($P < 0.0001$).

These findings support the antioxidant potential of UDC-Fer-Me, as shown by its ability to significantly reduce ROS production in neuronal cells, even at the lowest concentration tested.

3.4. Uptake of UDC-Fer-Me in respiratory nasal mucosa RPMI 2650 cells

3.4.1. Evaluation of UDC-Fer-Me potential toxicity on respiratory nasal mucosa RPMI 2650 cells

To assess the potential cytotoxicity of the prodrug on nasal mucosa, an MTT colorimetric assay was performed on RPMI 2650 cells exposed to various concentrations of UDC-Fer-Me (1, 5, 10, 40, 70, and 100 μM) as a pure compound. No cytotoxic effects were observed at any of the tested concentrations (1–100 μM; Fig. S3). Based on these findings, a concentration of 100 μM UDC-Fer-Me was subsequently selected for the uptake assay in RPMI 2650 cells.

3.4.2. Intracellular UDC-Fer-Me uptake by RPMI 2650 cells

After one day of adhesion from seeding, RPMI 2650 cells were incubated with 100 μM UDC-Fer-Me in complete culture medium for 10, 30, or 60 min at 37 °C to quantify the compound's cellular uptake and to monitor the appearance of its hydrolysis products, Fer-Me and Fer. As shown in Fig. 6, UDC-Fer-Me successfully permeated the RPMI cells, reaching intracellular concentrations of 3.95 ± 0.61 nmol/10^6 cells after 10 min and 4.59 ± 0.49 nmol/10^6 cells after 60 min of incubation.

In addition, Fer-Me, released as a hydrolysis product of UDC-Fer-Me, was detected intracellularly in RPMI cells at concentrations of 3.54 ± 0.14 nmol/10^6 cells and 4.13 ± 0.20 nmol/10^6 cells after 10 min and 60 min, respectively. Conversely, no intracellular Fer was detected within 60 min of incubation. These results demonstrate the ability of RPMI cells to hydrolyze the prodrug, with cleavage of the ester bond linking UDCA and Fer-Me representing the primary hydrolytic pathway (Fig. 1), whereas further conversion of Fer-Me to Fer appears limited under these conditions. No precipitated or sedimented prodrug was detected in cell-free wells, indicating the absence of extracellular residual compound.

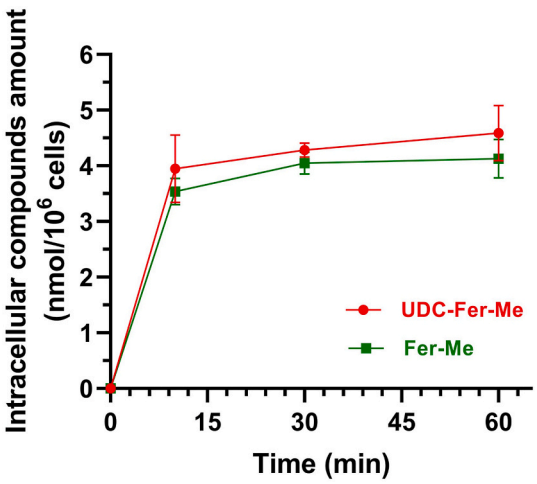

Fig. 6. Time-dependent intracellular amounts (nmol/10^6 cells) of UDC-Fer-Me (red) and its hydrolysis product Fer-Me (green) in RPMI 2650 cells after incubation with 100 μM UDC-Fer-Me (58.28 μg/mL) dissolved in complete A-MEM at 37 °C. Data are expressed as mean ± S.E.M. of four independent experiments. (For interpretation of the references to color in this figure legend, the reader is referred to the Web version of this article.)

3.5. Characterization of compritol-based SLNs

3.5.1. Morphological analysis of the SLNs

Both unloaded and UDC-Fer-Me-loaded SLNs exhibited an irregular spherical morphology, with particle sizes on the order of 0.1 μm, especially for the loaded SLNs, as shown by the SEM micrographs in Fig. 7.

3.5.2. SLN size distribution analysis

Estimating the mean size and associated size distribution through SEM observations requires the acquisition of photographs rich in particles well separated from each other, so as to ensure a statistically relevant evaluation through the use of appropriate software. An alternative way to obtain the same information is to use techniques that directly analyze the suspensions as they are to guarantee the measurement of an adequate number of particles and avoid possible modifications.

Among the methods routinely used, DLS is widely recognized as fast and user-friendly approach, providing low-resolution and semi-quantitative size distributions, albeit with good statistical sampling. DLS measurements confirm that the incorporation of UDC-Fer-Me during SLN formulation promoted the formation of a numerically significant population of small particles (~100 nm; Fig. 8 and Fig. S4) along with a second relevant population of larger particles (~400 nm; red line). The presence of aggregates is reflected by the Z-average and PDI values (Table 1). In contrast, unloaded SLNs show a single-size population of approximately 200 nm, with a PDI value which suggests also for this sample a size heterogeneity (Table 1).

While DLS is ideal for monodisperse particles, CFFF is excellent for complex, polydisperse, and aggregated samples, as it would seem this case. Fig. 9 reports the CFFF particle size distributions elaborated from the UV signal, acquired as a function of retention time (fractograms) [42] (Fig. S5). Both unloaded and loaded samples appear high polydispersed, with particles and aggregates ranging between 60 nm up to 1500 nm, with average sizes peaking at 400 and 500 nm, respectively. In agreement with the DLS data, the presence of the drug seems to generate a small population of about 150 nm (red line). The slight discrepancy observed in the main peak position (400 nm vs 500 nm of the unloaded SLNs) could be ascribed to a difference in the density of unloaded versus loaded particles, which were not accounted for in the CFFF data processing (assumed particle density $\rho_p = 1.06$ g/mL for both).

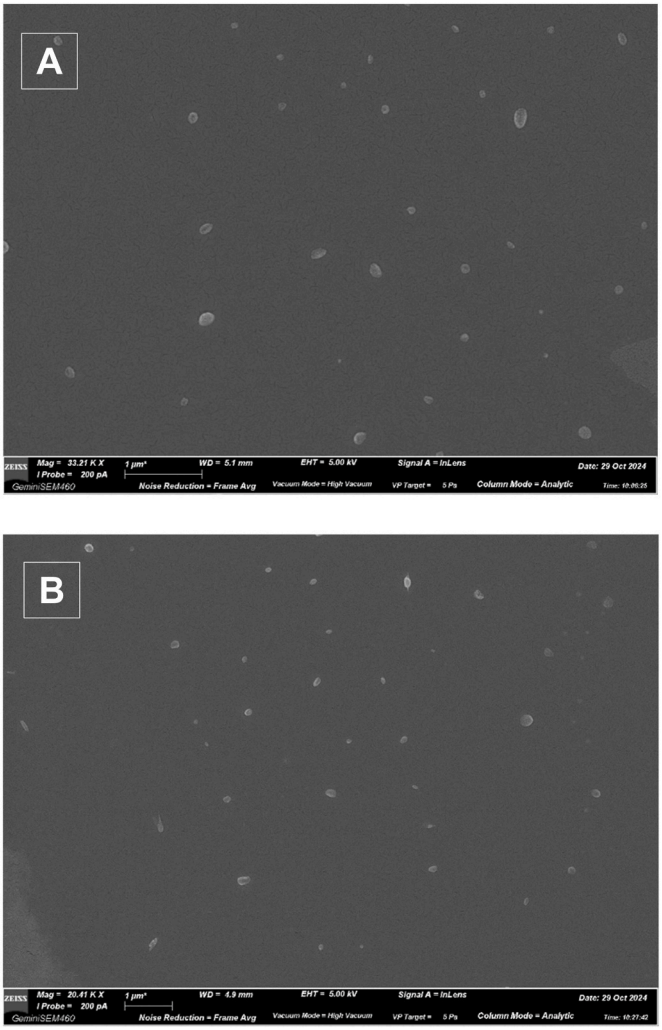

Fig. 7. Scanning electron microscopy (SEM) micrographs of the SLNs based on compritol. **(A)** Unloaded SLNs. **(B)** UDC-Fer-Me-loaded SLNs.

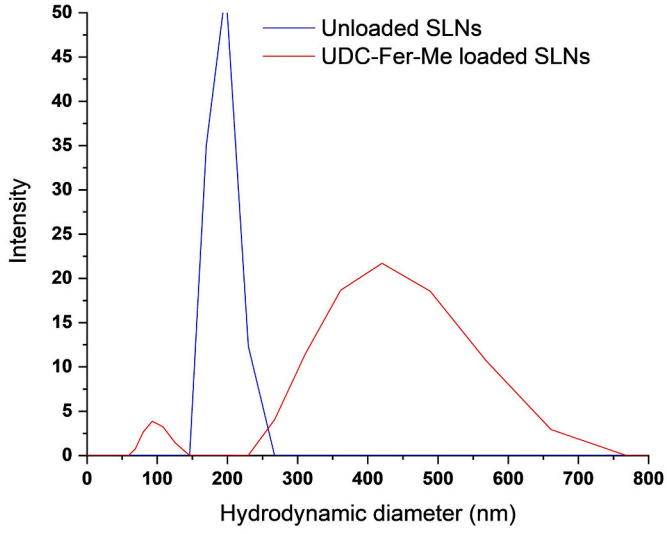

Fig. 8. DLS intensity particle size distributions for unloaded SLNs and UDC-Fer-Me-loaded SLNs.

Table 1
Intensity-weighted mean hydrodynamic size (Z-average), Polydispersity Index (PDI) and Zeta potential (ζ) of UDC-Fer-Me-loaded and unloaded SLNs.

System	Z-average (nm)	PDI	ζ potential (mV)
UDC-Fer-Me-loaded SLNs	594 ± 24	0.536 ± 0.210	−36.56 ± 0.76
Unloaded SLNs	192 ± 12	0.422 ± 0.199	−33.21 ± 0.84

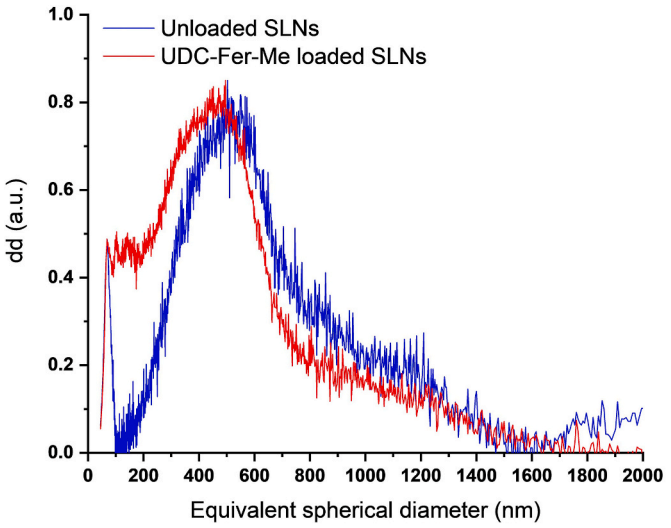

Fig. 9. Particle size distributions of the unloaded SLNs and UDC-Fer-Me-loaded SLNs elaborated from the CFFF fractograms (see Fig. S6).

3.5.3. *Analysis of the UDC-Fer-Me content in the SLNs*

The UDC-Fer-Me content was quantified in terms of drug loading (DL %) and encapsulation efficiency (EE%) after freeze-drying, as described in section 2.11.3. Specifically, the amount of prodrug encapsulated in the compritol-based SLNs (DL%) was found to be 7.95 ± 0.46%, corresponding to an encapsulation efficiency (EE%) of 61.01 ± 3.54%.

3.5.4. *Differential scanning calorimetry analysis of the SLNs*

A DSC analysis was performed to investigate the potential interactions between the compritol lipid matrix and the UDC-Fer-Me prodrug in the SLNs. In the DSC curve of pure compritol powder a single endothermic signal is visible, related to the melting process (Fig. 10A), with onset temperature T_O = (68.5 ± 0.3) °C and enthalpy ΔH_m = (124 ± 2) J/g (Table 2). T_O was evaluated using the extrapolation method [43]. The DSC signal of pure UDC-Fer-Me showed an exothermic peak with onset at ~85 °C, most likely related to a disorder/order transition (Fig. 10B), while the melting process is actually not detectable, indicating an almost negligible melting enthalpy.

In unloaded SLNs, the melting process gave rise to a double-peak signal, which is due to the interaction of compritol with surfactant residues (Fig. 10C, blue line). Both T_O and ΔH_m are decreased, compared to the values for pure compritol (Table 2). This could be traced back to the nanometric size of the SLNs (section 3.5) and to the presence of surfactant residues [44].

The DSC signal of UDC-Fer-Me-loaded SLNs is similar to that of the unloaded SLNs (Fig. 10C, red line), but reduced values of both T_O and ΔH_m were measured (Table 2). To explain these results, we carried out DSC analysis on a physical mixture of compritol (80 % (w/w)) and UDC-Fer-Me (20 % (w/w)) powders.

During the first measurement run (Fig. 10D, orange line), T_O was equal, within experimental error, to that of pure compritol and ΔH_m ~99 J/g (Table 2), corresponding to the contribution provided solely by the compritol fraction. These findings indicate that, in the physical mixture, no significant interaction occurred between the drug and the lipid phase. During the second measurement run (Fig. 10D, green line),

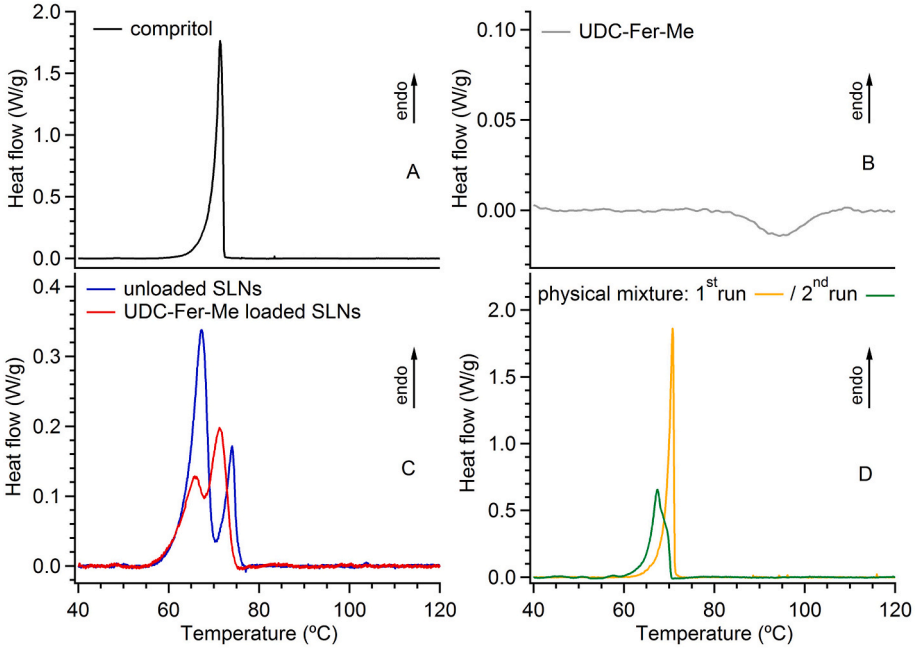

Fig. 10. DSC curves collected on: **(A)** pure compritol, **(B)** pure UDC-Fer-Me, **(C)** SLNs, unloaded (blue straight line) and loaded with UDC-Fer-Me (red straight line), **(D)** compritol (80 % (w/w)) and UDC-Fer-Me (20 % (w/w)) physical mixture during the 1st run of measurement (orange line) and the 2nd run (green line). (For interpretation of the references to color in this figure legend, the reader is referred to the Web version of this article.)

Table 2
Melting onset temperature T_O and melting enthalpy ΔH_m for pure compritol, unloaded and UDC-Fer-Me loaded SLNs, and for the UDC-Fer-Me/compritol physical mixture. All data are expressed as the mean ± S.E.M.

Compound		T_O (°C) (±0.3 °C)	ΔH_m (J/g) (±2 J/g)
pure compritol		68.5	124
unloaded SLNs		62.7	59
UDC-Fer-Me-loaded SLNs		59.7	44
UDC-Fer-Me/compritol physical mixture	1st run	68.4	99
	2nd run	64.4	74

both T_O and ΔH_m were lower compared to those observed in the first run. This can be explained by considering that, at the end of the first run, both compritol and UDC-Fer-Me had melted, and the lipophilicity of UDC-Fer-Me likely promoted intermixing between the two components of the physical mixture. Therefore, referring back to the results in Fig. 10C, the reduced T_O and ΔH_m values observed in the UDC-Fer-Me–loaded SLNs, compared with the unloaded ones, can be interpreted as a clear indication of an effective dispersion of the prodrug within the SLNs. The presence of the prodrug in the compritol matrix is expected to alter the molecular configuration of the latter, changing its density, as also inferred from the results on the SLNs size distribution, shown in section 3.5.2.

3.6. Dissolution of UDC-Fer-Me and release studies from SLNs

The dissolution studies of UDC-Fer-Me and the analysis of its release from the SLNs were performed at 37 °C in a mixture of H_2O and MeOH (50:50, v/v). The inclusion of MeOH in the medium was necessary due to the strong insolubility of UDC-Fer-Me in water (see section 3.1). Specifically, the H_2O/MeOH mixture allowed the experiments to be conducted under sink conditions by using a total UDC-Fer-Me concentration of 11.6 μg/mL (20 μM) in the medium containing either the raw compound or the UDC-Fer-Me-loaded particles. This concentration corresponds to approximately 10% of its solubility in this solvent system (section 3.1). Alternatively, to evaluate the dissolution and release patterns of UDC-Fer-Me in a physiological-like environment, the measurements were further conducted in 10 mM acetate buffer (pH 5.5) supplemented with 0.1% BSA and 0.05% sodium taurocholate as solubilizing agents alternative to MeOH. In this case the experiment was conducted by using a total UDC-Fer-Me concentration of 3.5 μg/mL (6 μM), corresponding to about 30% of saturation concentration (section 3.1) in the acetate buffer described above, incubating either the raw compound or the UDC-Fer-Me-loaded SLNs.

Before evaluating dissolution and release, a 10 μM UDC-Fer-Me solution (5.8 μg/mL) in the H_2O/MeOH mixture (50:50, v/v) and a 3 μM UDC-Fer-Me solution in 10 mM acetate buffer (pH 5.5) supplemented with 0.1% BSA and 0.05% sodium taurocholate were prepared directly from its DMSO stock solution and used for stability testing. These stability studies confirmed the complete absence of UDC-Fer-Me degradation over 8 h of incubation at 37 °C in both systems.

As shown in Fig. 11, the apparent release profile of UDC-Fer-Me from the loaded SLNs was compared with the apparent dissolution profile of the raw prodrug powder. In H_2O/MeOH 50:50 v/v mixture, UDC-Fer-Me exhibited a relatively poor intrinsic dissolution rate, with only about 37% of the total amount dissolved after 6 h of incubation. Under the same conditions, the apparent release from the SLNs was characterized by a rapid burst effect, with approximately 90% of the UDC-Fer-Me released within 5 min, and complete dissolution achieved within 20 min.

The absence of methanol in the 10 mM acetate buffer (pH 5.5) supplemented with 0.1% BSA and 0.05% sodium taurocholate sensibly reduced the dissolution rate of UDC-Fer-Me, allowing only ~5% of the total amount to be dissolved within 6 h of incubation (Fig. 11). Nevertheless, the apparent release in this medium of the prodrug from the SLNs was characterized by a pattern that allowed its dissolution to complete within 45 min of incubation (Fig. 11).

These results appear highly promising for nasal administration and subsequent brain targeting.

3.7. Intravenous administration of UDC-Fer-Me to rats (in vivo studies)

The prodrug behavior of UDC-Fer-Me was also investigated *in vivo*, following its intravenous administration to rats, with pharmacokinetic analysis performed in the bloodstream and CSF. Fig. 12 reports the UDC-

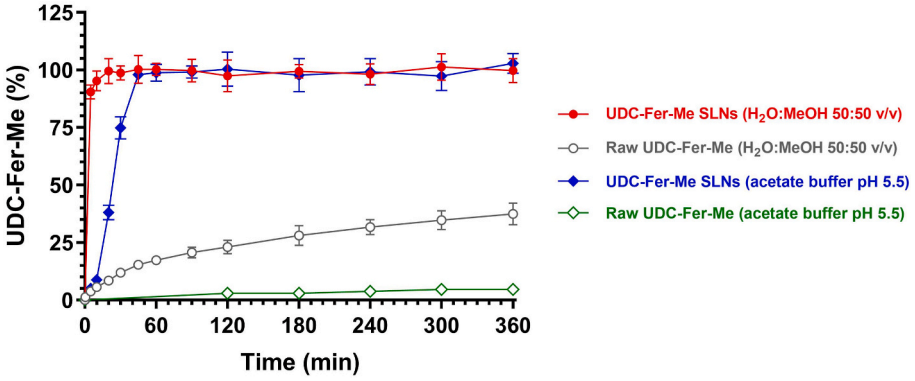

Fig. 11. *In vitro* release of UDC-Fer-Me from the compritol-based SLNs (UDC-Fer-Me SLNs) in a mixture of H_2O and MeOH 50:50 v/v or in a 10 mM acetate buffer (pH 5.5) supplemented with 0.1% BSA and 0.05% sodium taurocholate. The release profiles are compared with those of the raw prodrug (Raw UDC-Fer-Me) dissolution over time. All data are reported as the mean ± S.E.M. of three independent experiments.

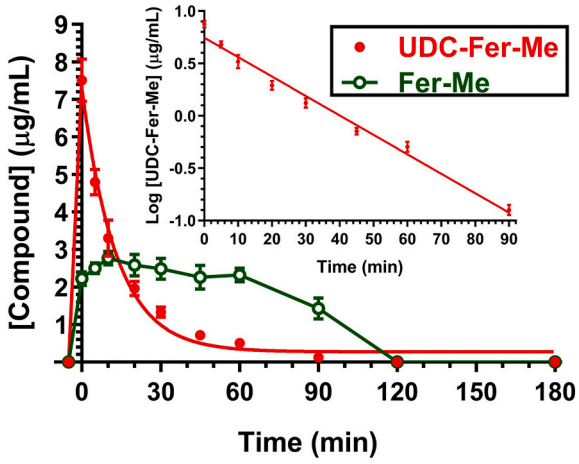

Fig. 12. Elimination profile of UDC-Fer-Me in the bloodstream after infusion to rats of 500 μg (2 mg/kg). A first order kinetic characterized the elimination, as confirmed by the semilogarithmic plot in the inset (n = 8, r = 0.991, $P < 0.0001$). The half-life of UDC-Fer-Me was calculated to be 16.7 ± 0.6 min. The Fer-Me profile obtained by the *in vivo* hydrolysis of UDC-Fer-Me is also represented. All data are reported as the mean ± S.E.M. of at least four independent experiments.

Fer-Me profile obtained in the bloodstream after the intravenous infusion of a 500-μg dose (2 mg/kg).

At the end of infusion, the UDC-Fer-Me plasmatic concentration was 7.5 ± 0.4 μg/mL (Table 3), and subsequently decreased over time, following an apparent first order kinetic, until the prodrug was no longer detectable within 120 min. The first-order kinetic elimination was confirmed by the linearity of the semilogarithmic plot reported in the inset of Fig. 12 (n = 8, r = 0.991, $P < 0.0001$), allowing calculation of k_{el} and $t_{1/2}$ values of 0.041 ± 0.002 min^{-1} and 16.7 ± 0.6 min, respectively.

Table 3
Intravenous administration to rats of 500 μg (2 mg/kg) of UDC-Fer-Me: half-life ($t_{1/2}$) detected in the bloodstream and its concentration at the end of infusion (C_{max} at t_{max} = 0). The highest concentration (C_{max}) of the prodrug hydrolysis product Fer-Me and its corresponding time (t_{max}) obtained in the bloodstream after the intravenous administration of UDC-Fer-Me are reported. The area under concentration (AUC) values of both compounds are also reported. All data are expressed as the mean ± S.E.M. of four independent experiments.

Compound	C_{max} (μg/mL)	t_{max} (min)	$t_{1/2}$ (min)	AUC (μg mL^{-1} min)
UDC-Fer-Me	7.5 ± 0.4	0	16.7 ± 0.6	148 ± 4
Fer-Me	2.8 ± 0.1	10	–	230 ± 8

The AUC value obtained after intravenous infusion of UDC-Fer-Me was 148 ± 4 μg mL^{-1} min (Table 3).

The *in vivo* hydrolysis of UDC-Fer-Me was shown by the appearance of Fer-Me in whole blood. Its concentrations ranged from 1.4 ± 0.2 to 2.8 ± 0.1 μg/mL (the C_{max} at 10 min, Table 3) between the end of infusion and 90 min, then decreased to undetectable levels within 120 min. The AUC value calculated for this profile was 230 ± 8 μg mL^{-1} min (Table 3).

Neither UDC-Fer-Me nor its metabolites were detected in the CSF after intravenous administration.

These results demonstrate that, following intravenous administration to rats, UDC-Fer-Me is eliminated through hydrolytic processes leading to the release of Fer-Me. Accordingly, UDC-Fer-Me can be regarded as a prodrug of both UDCA and Fer-Me *in vivo*. The absence of detectable Fer in the bloodstream profiles reported in Fig. 12 further indicates that, as previously observed in rat liver and brain homogenates, the hydrolysis of the ester bond linking UDCA and Fer-Me predominates over the hydrolysis of the methyl-ester group, as illustrated in the scheme shown in Fig. 1.

3.8. Nasal administration of UDC-Fer-Me

UDC-Fer-Me was nasally administered to rats at the dose of 2 mg/kg (500 μg) as an aqueous suspension of the raw prodrug. Under these conditions, neither UDC-Fer-Me nor its hydrolysis products were detected in the bloodstream or CSF within 6 h. In contrast, intranasal administration of the same dose of UDC-Fer-Me encapsulated in compritol-based SLNs enabled detection of both the prodrug and its hydrolysis product Fer-Me in the bloodstream and CSF. In particular, as reported in Fig. 13A, UDC-Fer-Me was detected in the bloodstream of rats 30 min after the administration with a concentration of 0.15 ± 0.04 μg/mL (0.26 ± 0.07 μM); C_{max} value of 1.21 ± 0.09 μg/mL (2.07 ± 0.15 μM) was reached at 45 min (t_{max}), after which concentrations declined to undetectable levels within 120 min. The AUC value of this profile was 48.4 ± 2.5 μg mL^{-1} min (Table 4), corresponding to a nasal bioavailability (F) of 32.7 ± 3.2%.

Fer-Me was also detected in the bloodstream of rats following nasal administration of the compritol-based SLNs (Fig. 13A). In particular, it was first measurable 45 min after administration at a concentration of 0.16 ± 0.02 μg/mL (0.75 ± 0.10 μM). Fer-Me levels then increased and remained around 0.4 μg/mL (≈1.9 μM) between 60 and 120 min, reaching a C_{max} value of 0.42 ± 0.05 μg/mL (2.03 ± 0.26 μM) at 120 min (Table 3), before declining to undetectable levels within 180 min. The corresponding AUC was 41.6 ± 2.8 μg mL^{-1}·min (Table 3).

After nasal administration of the SLNs, UDC-Fer-Me was also detected in the CSF of rats (Fig. 13B). Its concentration increased rapidly after administration, reaching a C_{max} of 1.8 ± 0.08 μg/mL (3.13 ± 0.14 μM) at

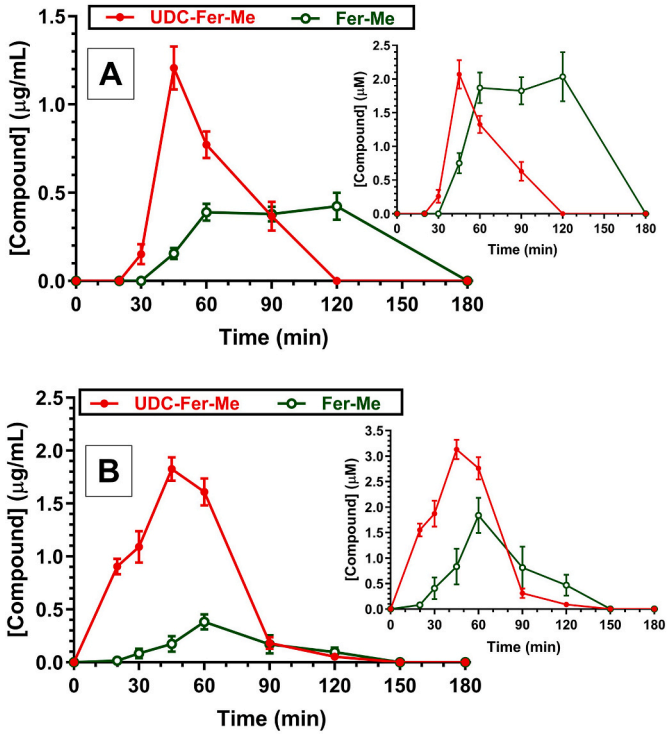

Fig. 13. Nasal administration to rats of UDC-Fer-Me (500 µg) loaded in compritol-based SLNs: profiles of the prodrug (UDC-Fer-Me) and its hydrolysis product Fer-Me in the bloodstream (**A**) and in the CSF (**B**). The insets report the µM concentrations of the compounds. All data are reported as the mean ± S.E.M. of at least four independent experiments.

45 min (t_{max}), then declined to undetectable levels within 150 min. The AUC for this profile was 97.8 ± 3.1 µg mL^{-1}·min (Table 3).

Fer-Me, the hydrolysis product of the prodrug, was likewise detected in the CSF after nasal administration of the SLNs (Fig. 13B). In this case, the C_{max} value (0.38 ± 0.05 µg/mL, equivalent to 1.84 ± 0.24 µM)was reached 60 min (t_{max}) after administration, and its concentration declined to zero within 150 min. The AUC for this profile was 20.5 ± 2.5 µg mL^{-1}·min (Table 3).

The ratios of AUC values between the CSF and bloodstream after nasal administration of the SLNs were 2.02 ± 0.16 for UDC-Fer-Me and 0.49 ± 0.09 for Fer-Me.

4. Discussion

Natural compounds such as Fer and UDCA have shown antioxidant properties that appear beneficial in the context of neuroprotection [6,45]. The antioxidant activity of Fer is attributed to its phenolic ring conjugated to the C3 side chain, which effectively terminates radical chain reactions by scavenging free radicals [46]. Importantly, Fer also helps to maintain mitochondrial dynamics [47], which are often disrupted under oxidative stress, leading to neuronal degeneration [48,49]. This property is shared by UDCA [8]. Although UDCA and Fer can cross the BBB, very high oral doses are required to overcome their pharmacokinetic limitations and achieve neuroprotective effects [12–15].

We have previously demonstrated that appropriately designed nasal formulations can enable the direct delivery of neuroactive agents or their prodrugs to the CNS [11,18,50]. Accordingly, this approach was applied to Fer and UDCA with the aim of achieving potential neuroprotective effects in the brain while potentially reducing the doses required compared to their separate oral administration.

The simultaneous intranasal administration of UDCA and Fer may be considered a form of "combination therapy", in which SLNs play a key role in enhancing the bioavailability of poorly water-soluble drugs [20]. However, the log $P_{o/w}$ value of Fer (~1.4, Table S1) is suboptimal for efficient encapsulation in lipid-based carriers [21]. In this context, a prodrug approach aimed at increasing drug hydrophobicity may represent an effective strategy to improve encapsulation efficiency. Indeed, we have previously applied this approach to enhance the incorporation of poorly lipophilic compounds, such as dopamine and an anti-ischemic agent, into lipid-based carriers [51,52]. A similar strategy has also been employed for geraniol to reduce its high volatility [18]. Furthermore, we demonstrated that a Fer prodrug, obtained as its methyl ester (Fer-Me), exhibited significantly improved encapsulation in solid lipid microparticles compared with the parent compound [21]. This effect was further enhanced using a methylated dimeric conjugate (Fer-Fer-Me) [11].

On the basis of the considerations outlined above, we designed and synthesized the prodrug UDC-Fer-Me (Fig. 1), obtained through ester conjugation of the methyl ester of Fer (Fer-Me) with UDCA. Fer-Me was selected because it retains the antioxidant properties of Fer [11], while enabling the design of a conjugate with increased hydrophobicity, a key feature for efficient encapsulation into SLNs intended for nose-to-brain delivery via nasal administration. The enhanced hydrophobicity of UDC-Fer-Me is supported by its calculated log $P_{o/w}$ value, which increases from ~1.7 (Fer-Me) to ~6 upon ester conjugation with UDCA (log P ~4; Table S1).

Following synthesis, UDC-Fer-Me was first evaluated as a prodrug in physiological environments. Using optimized extraction procedures and HPLC-UV methods, we quantified UDC-Fer-Me and its hydrolysis products (Fer-Me and Fer; Fig. 1) in rat liver and brain homogenates. UDCA does not possess a chromophore suitable for quantification by UV spectroscopy, therefore the detection of Fer-Me in these biological matrices was considered indicative of cleavage of the ester bond linking UDCA and Fer-Me, leading to release of the two moieties. In addition to that of UDCA and Fer, the release of Fer-Me can be considered relevant for a possible therapeutic application taking into account that this compound retains the antioxidant properties of Fer [11] and can be further hydrolyzed to Fer (Fig. 1).

UDC-Fer-Me was stable in Tris-HCl buffer but was rapidly hydrolyzed in rat liver homogenate: within 10 min, ~90% of the prodrug was degraded, releasing ~75% Fer-Me and ~15% Fer. These findings indicate that cleavage of the UDC-Fer-Me ester bond is the dominant reaction, followed by slower hydrolysis of Fer-Me to Fer (Fig. 3A). Overall, these results suggest that, at the peripheral level, UDC-Fer-Me behaves as a prodrug of UDCA, Fer-Me, and Fer. In rat brain homogenate, UDC-Fer-Me was almost completely hydrolyzed within 180 min, releasing Fer-Me but not Fer (Fig. 3B), consistent with previous data on Fer-Me stability [11]. Therefore, at the central level, UDC-Fer-Me can be

Table 4
Nasal administration to rats of 500 µg (2 mg/kg) of UDC-Fer-Me encapsulated in compritol-based SLNs: the highest concentrations (C_{max}), their corresponding times (t_{max}) and the AUC values obtained in the bloodstream and cerebrospinal fluid (CSF) for this compound and its hydrolysis product Fer-Me are reported. All data are expressed as the mean ± S.E.M. of four independent experiments.

Compound	Body compartment	C_{max} (µg/mL)	C_{max} (µM)	t_{max} (min)	AUC (µg mL^{-1} min)
UDC-Fer-Me	bloodstream	1.21 ± 0.09	2.07 ± 0.15	45	48.4 ± 2.5
Fer-Me	bloodstream	0.42 ± 0.05	2.03 ± 0.26	120	41.6 ± 2.8
UDC-Fer-Me	CSF	1.83 ± 0.08	3.13 ± 0.14	45	97.8 ± 3.1
Fer-Me	CSF	0.38 ± 0.05	1.84 ± 0.24	60	20.5 ± 2.5

regarded as a prodrug of UDCA and Fer-Me. The ability to release Fer-Me in the brain can be considered significant, given its preserved antioxidant activity [11]. According to results obtained in rat and brain homogenates, UDC-Fer-Me can be defined as a mutual prodrug of UDCA and Fer-Me [53,54].

Taking into account these aspects and hypothesizing a nose-to-brain delivery of UDC-Fer-Me, we further assessed whether UDC-Fer-Me allows to induce antioxidant activity by testing its effects in neuronal differentiated Neu-2A cells exposed to oxidative stress (H_2O_2). Before conducting these tests, UDC-Fer-Me was shown to be non-toxic and to promote cell viability at concentrations ranging from 5 to 100 μM (Fig. 4). The increase in cell viability observed in the MTT assay should not be interpreted as a direct increase in cell number, but rather as an indication of enhanced mitochondrial metabolic activity in the existing neuronal cells. This effect suggests that UDC-Fer-Me, starting at concentrations of 5 μM, may exert a protective or stimulatory action on neuronal metabolism, rather than causing any toxicity. Such an effect is consistent with the known antioxidant properties of both UDCA and Fer derivatives, which are able to mitigate basal oxidative stress and improve mitochondrial efficiency. Accordingly, UDC-Fer-Me significantly reduced ROS production induced by H_2O_2 (Fig. 5), showing a similar antioxidant activity among the concentrations tested (1-10 μM). It is suggested that the lowest concentration assessed (1 μM) may trigger the peak intracellular antioxidant response, leading to a plateau where additional increases in compound concentration do not amplify the observed effect. A similar phenomenon was observed in Neu-2A cells exposed to H_2O_2 and treated with a recognized antioxidant compound, Urolithin A, which markedly decreased ROS production in comparison to H_2O_2 alone, although not in a concentration-dependent fashion [55]. Moreover, we cannot currently determine whether the antioxidant activity is due to the prodrug itself or its hydrolysis products. Nevertheless, the kinetic studies conducted in rat brain homogenate (Fig. 3B), suggest that UDC-Fer-Me undergoes hydrolysis within neuronal cells. Consequently, the antioxidant activity observed in differentiated Neuro-2A cells may be due to the intracellular hydrolysis of the prodrug, which leads to the release of Fer-Me and UDCA, both of which have independently shown neuroprotective and antioxidant properties in neuronal cell models. Specifically, Fer-Me maintains antioxidant activity that is comparable to that of the parent compound Fer [21], while UDCA has been demonstrated to inhibit ROS accumulation and protect mitochondrial function in Neuro-2A cells [8]. However, if the observed antioxidant activity was attributable to the prodrug itself, it did not show any cytotoxicity in the cell viability assays nor any pro-oxidant effects in the ROS assay. These findings therefore suggest that, if able to reach the CNS, the prodrug itself may exert protective effects before hydrolysis and release of UDCA and Fer-Me, potentially contributing to sustained activity. In contrast, we previously showed that a prodrug derived from Fer and geraniol decreased Neu-2A viability and increased ROS production under similar conditions [30], highlighting how conjugation of two compounds may drastically alter their biological properties. This does not appear to be the case of UDC-Fer-Me, which retained the beneficial effects of parent compounds.

To further investigate the UDC-Fer-Me prodrug behavior, its pharmacokinetics were as evaluated following intravenous administration to rats (Fig. 12). These studies revealed that UDC-Fer-Me reached a peak plasma concentration of ~8 μg/mL (~14 μM) and was eliminated within 120 min, accompanied by release of Fer-Me (up to ~3 μg/mL, ~14 μM) (Fig. 12). These data indicate that, *in vivo*, UDC-Fer-Me undergoes hydrolysis at the ester conjugation site, leading to the release of UDCA and Fer-Me into the bloodstream. It should be noted that the interpretation of the *in vivo* pharmacokinetic profile of UDC-Fer-Me is limited by the lack of complementary *in vitro* stability studies in whole blood. Such experiments could provide additional insight into the contribution of blood components (*e.g.*, enzymes and plasma proteins) to the hydrolysis and stability of the prodrug. Therefore, although the observed plasma profiles suggest rapid hydrolysis of UDC-Fer-Me, the potential influence of other processes, including biodistribution, protein binding, and clearance, cannot be excluded. Further investigations will be necessary to better elucidate the relative contribution of these factors.

We have previously reported that Fer-Me can be further hydrolyzed to Fer in rat whole blood [21]; however, following the intravenous administration of UDC-Fer-Me, Fer was not detected in the rats' bloodstream. This finding suggests that, *in vivo*, the elimination rate of Fer-Me is not substantially lower than its hydrolysis rate, which is consistent with previous pharmacokinetic data on this compound [50]. Concerning the concentrations measured in rat blood after intravenous infusion of the prodrug (up to 14 μM), it is worth noting that levels up to 30 μM of UDCA or Fer, achieved after oral administration, are considered well tolerated in both humans and rats [12,56].

Intravenous administration of UDC-Fer-Me did not allow detection of the prodrug or its hydrolysis products, Fer-Me and Fer, in the CSF of rats. This result indicates that the prodrug was not detectable in the CNS under the tested conditions, suggesting limited CNS availability in contrast to Fer and UDCA themselves [11,12]. However, no definitive conclusions on its ability to cross the blood–brain barrier can be drawn, as other factors (e.g., the relatively low administered dose and the sensitivity limits of the analytical method) cannot be excluded. The absence of UDC-Fer-Me metabolites detection in the CSF of rats appears moreover in good agreement with the very limited ability of Fer-Me to permeate into the CNS described in previous pharmacokinetic studies [11]. The limited ability of UDC-Fer-Me to cross physiological barriers between the bloodstream and the CNS may be inferred by comparison with another Fer-based prodrug, its methylated ester dimer (Fer--Fer-Me). In particular, following intravenous administration to rats at a dose of 1 mg/kg (i.e., half the dose used for UDC-Fer-Me), Fer-Fer-Me was detectable in the CSF, reaching concentrations up to 0.20 μg/mL [11]. This observation highlights that different prodrugs derived from the same parent compound may interact differently with transport proteins expressed at the physiological barriers between the blood and the CNS. Several prodrugs actively transported by carrier-mediated transporters were proposed for the uptake in the brain of neuroactive agents [57–61]; alternatively, specific prodrugs have been designed to evade or inhibit active efflux transporters at the blood-brain barrier [62–64].

Therefore, in this case, the nasal administration of UDC-Fer-Me represents a promising strategy for its potential delivery to the CNS. To explore this possibility, we investigated the ability of the prodrug to permeate nasal mucosal cells, considering that permeation across the olfactory mucosa is one of the main mechanisms by which compounds can reach the CSF following nasal administration [65,66]. UDC-Fer-Me did not alter the viability of nasal mucosa RPMI 2650 cells when incubated at concentrations ranging from 1 to 100 μM (Fig. S3). Similarly, a prodrug obtained by conjugation of Fer and Fer-Me did not impair the viability of neuronal-differentiated PC12 cells compared with untreated controls [11]. These findings further suggest that the increase in viability observed in Neu-2A cells may be cell-type dependent. The highest concentration of UDC-Fer-Me (100 μM) used for cell viability studies was selected for subsequent uptake studies in RPMI 2650 cells. Permeation studies (Fig. 6) demonstrated that (*i*) UDC-Fer-Me is able to permeate nasal mucosa RPMI 2650 cells, and (*ii*) these cells are able to hydrolyze the prodrug at the ester bond linking UDCA and Fer-Me but not to further hydrolyze Fer-Me to Fer. Indeed, after 1 h of incubation, equivalent molar amounts of UDC-Fer-Me and Fer-Me (up to about 4.5 nmol/10^6 cells) were detected intracellularly, indicating that UDC-Fer-Me is a promising candidate for nose-to-brain delivery. On the other hand, nasal administration of a water suspension of raw UDC-Fer-Me to rats did not allow detection of the prodrug or its hydrolysis products in either CSF or bloodstream. This result is not surprising given the compound's extremely poor water solubility (section 3.1), which likely prevented sufficient dissolution in the nasal cavity to enable permeation across the nasal mucosa. To overcome this limitation, a new nasal formulation was developed to significantly enhance the

dissolution rate of UDC-Fer-Me. Microparticulate or nanoparticulate systems based on stearic acid or compritol have been reported to markedly improve the dissolution rate of highly lipophilic prodrugs of neuroactive agents, thereby providing effective nasal formulations for nose-to-brain delivery [11,18,36,67]. In this study, we focused on compritol, a biocompatible glyceride widely used as a lipid carrier for nanoparticles [68]. Compritol enabled the preparation of SLNs with satisfactory UDC-Fer-Me loading (about 8%, section 3.5.3), irregular spherical morphology, with sizes in the 100 nm order of magnitude, evidenced by SEM micrographs (section 3.5.1). The PDI values ranged from 0.42 to 0.54 for unloaded and UDC-Fer-Me-loaded SLNs, respectively, indicating the tendency of these samples to aggregate, according to the data obtained by the CFFF measurements. The ζ potential values were ~ −35 mV for loaded and unloaded SLNs, suggesting their physical stability as nanodispersions [69]. Lipid carriers exhibit in general negatively charged surfaces [70,71]; the presence of non-ionic surfactants, such as Tween 80, and ionic surfactants, such as bile salts, can have contributed to making relatively high the ζ potential absolute value of the SLNs [18,70–73]. DSC analysis data suggested a good dispersion of the prodrug within the lipid matrix (section 3.5.4). A comparison of the apparent dissolution profile of raw UDC-Fer-Me with its apparent release from loaded SLNs in aqueous media demonstrated the ability of the nanoparticles to induce a very fast release of the prodrug in H_2O/MeOH 50:50 v/v mixture (Fig. 11). The use of 50% MeOH as a co-solvent was necessary to ensure adequate solubility of the lipophilic prodrug and maintain sink conditions at a concentration suitable for the subsequent HPLC quantification. In order to evaluate the dissolution and release patterns of UDC-Fer-Me in a physiological-like environment, an alternative medium was chosen, considering that the human nasal mucosa typically exhibits a physiological pH of 6.3 and nasal formulations are generally maintained within a pH range of 4.5 to 6.5 in order to minimize the risk of nasal irritation [19,74]. The dissolution and release measurements were therefore performed also in 10 mM acetate buffer (pH 5.5) supplemented with 0.1% BSA and 0.05% sodium taurocholate as solubilizing agents alternative to MeOH [75,76]. The sodium taurocholate concentration used was below its critical micellar concentration (CMC, 3-15 mM [77]), ensuring that the observed release reflects genuine drug diffusion from the lipid matrix rather than solvent- or micelle-driven extraction. The patterns obtained in the absence of methanol in the incubation medium are characterized by slower dissolution and release of the prodrug, even if the SLNs evidenced the ability to induce a release of the prodrug definitely faster than the dissolution rate of its raw form (Fig. 11). The fast release of UDC-Fer-Me from the SLNs may be attributed to a highly porous structure induced by a good dispersion of the prodrug within the lipid matrix, from which it is facilitated to dissolve in a dispersion medium. On the other hand, the dissolution profiles reported in Fig. 11 may suggest the prodrug localization on the nanocarrier's particle surface as a so-called drug-enriched shell model, even if this type of distribution is generally produced by hot homogenization techniques [78]. Further investigations are required to elucidate these aspects.

According to their release patterns, the SLNs appeared highly suitable for nasal administration to promote effective nose-to-brain delivery of UDC-Fer-Me. In this context, the rapid dissolution of UDC-Fer-Me in aqueous environments is likely an essential key to facilitate its permeation across the nasal mucosa [11]. Accordingly, following nasal administration of SLN encapsulated UDC-Fer-Me (2 mg/kg; 500 μg/rat), both the prodrug and its hydrolysis product, Fer-Me, were detected in the bloodstream and in the CSF of rats. In particular, UDC-Fer-Me reached in the bloodstream a C_{max} of 1.21 ± 0.09 μg/mL (2.07 ± 0.15 μM) at 15 min (Fig. 13), corresponding to an absolute bioavailability of approximately 30%. This result is consistent with the well-documented ability of nasally administered compounds to permeate the respiratory mucosa and enter the systemic circulation [65,79]. Fer-Me was also detected in the bloodstream, reaching peak molar concentrations after nasal administration comparable to those of UDC-Fer-Me (about 2 μM, Fig. 13). The presence of Fer-Me in the bloodstream can be attributed to hydrolysis of the prodrug by nasal mucosa cells (as described in section 3.4.2, Fig. 6) and potentially followed by additional hydrolysis occurring in the bloodstream (Fig. 12). Importantly, the nasal administration of SLNs also allowed detection of UDC-Fer-Me and Fer-Me in the CSF of rats. The prodrug reached a C_{max} of approximately 1.8 μg/mL, corresponding to about 3 μM. Notably, after nasal administration, UDC-Fer-Me maintained concentrations above 1 μM in the CSF for at least 1 h. These levels suggest that the prodrug may reach pharmacologically relevant concentrations in the CNS, potentially enabling antioxidant effects consistent with the *in vitro* findings (section 3.3.2, Fig. 5). Finally, the presence of Fer-Me, generated by hydrolysis of UDC-Fer-Me in olfactory mucosa cells (Fig. 6) and possibly within the CNS (as suggested by the results in rat brain homogenates, Fig. 3B), may further contribute, together with UDCA, to the overall neuroprotective potential of the prodrug.

These *in vivo* results indicate that the SLNs can promote the UDC-Fer-Me bioavailability after nasal administration, despite their negative ζ potential values interfere by electrostatic repulsions with adhesion to mucosal membranes, which are characterized by the presence of negatively charged species [80]. On the other hand, other nanoparticulate systems characterized by relatively strong negative ζ potential values were previously evidenced to induce satisfactory uptake of prodrugs in the CSF of rats after nasal administration [18,73]. Compritol-based nanoformulations have been reported to be optimized for their mucoadhesion by coating with chitosan or by incorporating them in thermosensitive mucoadhesive systems [69,81,82], suggesting further improvement strategies for the UDC-Fer-Me loaded SLNs here described.

5. Conclusions

We developed and characterized a novel prodrug (UDC-Fer-Me) designed to deliver both UDCA and Fer to the CNS via nasal administration. UDC-Fer-Me was efficiently hydrolyzed in physiological environments to release UDCA and Fer-Me, exhibited antioxidant activity in neuronal cells. Moreover, the dissolved form of this prodrug appeared able to permeated nasal mucosa cells, but, owing to its poor aqueous solubility, direct nasal delivery as water suspension form was precluded. On the other hand, encapsulation of the prodrug in compritol-based SLNs enabled its CNS exposure *in vivo* after intranasal administration, as demonstrated by measurable levels of UDC-Fer-Me and Fer-Me in CSF.

Overall, these findings suggest that UDC-Fer-Me-loaded SLNs can be a promising non-invasive strategy for the delivery of antioxidant agents to the CNS, with the goal of promoting neuroprotection.

Ethics approval

The experimental procedures performed with the rats were approved by the Italian Ministry of Health and performed in accordance with the European Communities Council Directive of September 2010 (2010/63/EU). According to the ARRIVE guidelines, all possible efforts were made to minimize animal pain and discomfort and to reduce the number of experimental subjects.

Funding

This work was financially supported by the University of Ferrara, Italy, in the frame of the projects FAR2022 (2022-FAR.L-DA_018, A.D), FAR2023 (2023-FAR.L_chimiche_DA, A.D.), and FIRD 2024 (L.D.B.).

CRediT authorship contribution statement

Giada Botti: Conceptualization, Data curation, Formal analysis, Investigation, Methodology, Validation, Visualization, Writing – original draft, Writing – review & editing. **Elena Marchesi:** Data curation,

Investigation, Writing – review & editing. **Luca Ferraro:** Data curation, Investigation, Methodology, Resources, Validation, Writing – review & editing. **Sarah Beggiato:** Data curation, Investigation, Methodology, Validation, Writing – review & editing. **Anna Bianchi:** Data curation, Investigation, Methodology, Validation, Writing – original draft, Writing – review & editing. **Barbara Pavan:** Conceptualization, Data curation, Formal analysis, Investigation, Methodology, Resources, Supervision, Validation, Visualization, Writing – original draft, Writing – review & editing. **Catia Contado:** Data curation, Investigation, Methodology, Validation, Visualization, Writing – original draft, Writing – review & editing. **Federico Spizzo:** Data curation, Investigation, Methodology, Validation, Visualization, Writing – original draft, Writing – review & editing. **Lucia Del Bianco:** Data curation, Funding acquisition, Investigation, Methodology, Validation, Visualization, Writing – original draft, Writing – review & editing. **Daniela Perrone:** Supervision, Writing – original draft, Writing – review & editing. **Alessandro Dalpiaz:** Conceptualization, Data curation, Formal analysis, Funding acquisition, Investigation, Methodology, Project administration, Resources, Supervision, Validation, Visualization, Writing – original draft, Writing – review & editing.

Declaration of competing interest

The authors declare that they have no known competing financial interests or personal relationships that could have appeared to influence the work reported in this paper.

Acknowledgment

The authors acknowledge the use of the instruments at the Electron Microscopy Center of the University of Ferrara and the scientific and technical assistance of Negar Eftekhari of the Department of Environmental and Prevention Sciences of the University of Ferrara (Italy).

Appendix A. Supplementary data

Supplementary data to this article can be found online at https://doi.org/10.1016/j.jddst.2026.108388.

Data availability

Data will be made available on request.

References

[1] F. Limanaqi, F. Biagioni, F. Mastroiacovo, M. Polzella, G. Lazzeri, F. Fornai, Merging the multi-target effects of phytochemicals in neurodegeneration: from oxidative stress to protein aggregation and inflammation, Antioxidants 9 (2020) 1022, https://doi.org/10.3390/antiox9101022.

[2] D.K. Yadav, Potential therapeutic strategies of phytochemicals in neurodegenerative disorders, Curr. Top. Med. Chem. 21 (2021) 2814–2838, https://doi.org/10.2174/1568026621666211201150217.

[3] L. Pogačnik, A. Ota, N.P. Ulrih, An overview of crucial dietary substances and their modes of action for prevention of neurodegenerative diseases, Cells 9 (2020) 576, https://doi.org/10.3390/cells9030576.

[4] B.K. Velmurugan, B. Rathinasamy, B.P. Lohanathan, V. Thiyagarajan, C.F. Weng, Neuroprotective role of phytochemicals, Molecules 23 (2018) 2485, https://doi.org/10.3390/molecules23102485.

[5] F. Hedayatikatouli, M. Kalyn, D. Elsaid, H.A. Mbesha, M. Ekker, Neuroprotective effects of ascorbic acid, vanillic acid, and ferulic acid in dopaminergic neurons of zebrafish, Biomedicines 12 (2024) 2497, https://doi.org/10.3390/biomedicines12112497.

[6] S. Hassani, A. Esmaeili, The neuroprotective effects of ferulic acid in toxin-induced models of Parkinson's disease: a review, Ageing Res. Rev. 97 (2024) 102299, https://doi.org/10.1016/j.arr.2024.102299.

[7] M.L. Huang, S. Chiang, D.S. Kalinowski, D.H. Bae, S. Sahni, D.R. Richardson, The role of the antioxidant response in mitochondrial dysfunction in degenerative diseases: cross-talk between antioxidant defense, autophagy, and apoptosis, Oxid. Med. Cell. Longev. 2019 (2019) 6392763, https://doi.org/10.1155/2019/6392763.

[8] H. Qi, D. Shen, C. Jiang, H. Wang, M. Chang, Ursodeoxycholic acid protects dopaminergic neurons from oxidative stress via regulating mitochondrial function, autophagy, and apoptosis in MPTP/MPP$^+$-induced Parkinson's disease, Neurosci. Lett. 741 (2021) 135493, https://doi.org/10.1016/j.neulet.2020.135493.

[9] C. Pacelli, N. Giguère, M.J. Bourque, M. Lévesque, R.S. Slack, L.É. Trudeau, Elevated mitochondrial bioenergetics and axonal arborization size are key contributors to the vulnerability of dopamine neurons, Curr. Biol. 25 (2015) 2349–2360, https://doi.org/10.1016/j.cub.2015.07.050.

[10] X. Flores-Ponce, I. Velasco, Dopaminergic neuron metabolism: relevance for understanding Parkinson's disease, Metabolomics 20 (2024) 116, https://doi.org/10.1007/s11306-024-02181-4.

[11] G. Botti, A. Bianchi, A. Dalpiaz, P. Tedeschi, V. Albanese, M. Sorrenti, L. Catenacci, M.C. Bonferoni, S. Beggiato, B. Pavan, Dimeric ferulic acid conjugate as a prodrug for brain targeting after nasal administration of loaded solid lipid microparticles, Expert Opin. Drug Deliv. 20 (2023) 1657–1679, https://doi.org/10.1080/17425247.2023.2286369.

[12] G.J. Parry, C.M. Rodrigues, M.M. Aranha, S.J. Hilbert, C. Davey, P. Kelkar, W. C. Low, C.J. Steer, Safety, tolerability, and cerebrospinal fluid penetration of ursodeoxycholic acid in patients with amyotrophic lateral sclerosis, Clin. Neuropharmacol. 33 (2010) 17–21, https://doi.org/10.1097/WNF.0b013e3181c47569.

[13] S.M. Grant, S. DeMorrow, Bile acid signaling in neurodegenerative and neurological disorders, Int. J. Mol. Sci. 21 (2020) 5982, https://doi.org/10.3390/ijms21175982.

[14] T. Payne, M. Sassani, E. Buckley, S. Moll, A. Anton, M. Appleby, S. Maru, R. Taylor, A. McNeill, N. Hoggard, C. Mazza, I.D. Wilkinson, T. Jenkins, T. Foltynie, O. Bandmann, Ursodeoxycholic acid as a novel disease-modifying treatment for Parkinson's disease: protocol for a two-centre, randomised, double-blind, placebo-controlled trial. The 'UP' study, BMJ Open 10 (2020) e038911, https://doi.org/10.1136/bmjopen-2020-038911, 10.

[15] O.M. Youssef, N.H. Lashine, M. El-Nablaway, M.I. El-Yamany, M.M. Youssef, D. A. Arida, Ferulic acid mitigated rotenone toxicity - evoked Parkinson in rat model by featuring apoptosis, oxidative stress, and neuroinflammation signaling, Tissue Cell 91 (2024) 02614, https://doi.org/10.1016/j.tice.2024.102614.

[16] L. Illum, Is nose-to-brain transport of drugs in man a reality? J. Pharm. Pharmacol. 56 (2004) 3–17, https://doi.org/10.1211/0022357022539.

[17] N.J. Johnson, L.R. Hanson, W.H., Frey trigeminal pathways deliver a low molecular weight drug from the nose to the brain and orofacial structures, Mol. Pharm. 7 (2010) 884–893, https://doi.org/10.1021/mp100029t.

[18] E.R. de Oliveira Junior, E. Truzzi, L. Ferraro, M. Fogagnolo, B. Pavan, S. Beggiato, C. Rustichelli, E. Maretti, E.M. Lima, E. Leo, A. Dalpiaz, Nasal administration of nanoencapsulated geraniol/ursodeoxycholic acid conjugate: towards a new approach for the management of Parkinson's disease, J. Contr. Release 321 (2020) 540–552, https://doi.org/10.1016/j.jconrel.2020.02.033.

[19] L.A. Keller, O. Merkel, A. Popp, Intranasal drug delivery: opportunities and toxicologic challenges during drug development, Drug Deliv. Transl. Res. 12 (4) (2022) 735–757, https://doi.org/10.1007/s13346-020-00891-5.

[20] J. Torres, R. Silva, G. Farias, J.M.S. Lobo, D.C. Ferreira, A.C. Silva, Co-encapsulation in solid lipid nanoparticles and nanostructured lipid carriers as an emerging therapeutic strategy, Mol. Diagn. Ther. 30 (2) (2026) 195–217, https://doi.org/10.1007/s40291-025-00821-6.

[21] G. Botti, A. Bianchi, B. Pavan, P. Tedeschi, V. Albanese, L. Ferraro, F. Spizzo, L. Del Bianco, A. Dalpiaz, Effects of microencapsulated ferulic acid or its prodrug methyl ferulate on neuroinflammation induced by muramyl dipeptide, Int. J. Environ. Res. Public Health. 19 (2022) 10609, https://doi.org/10.3390/ijerph191710609.

[22] A. Daina, O. Michielin, V. Zoete, SwissADME: a free web tool to evaluate pharmacokinetics, drug-likeness and medicinal chemistry friendliness of small molecules, Sci. Rep. 7 (2017) 42717, https://doi.org/10.1038/srep42717.

[23] O.H. Lowry, N.J. Rosebrough, A.L. Farr, R.J. Randall, Protein measurement with the Folin phenol reagent, J. Biol. Chem. 193 (1951) 265–275, https://doi.org/10.1016/s0021-9258(19)52451-633.

[24] K. Felgenhauer, Protein size and cerebrospinal fluid composition, Klin. Wochenschr. 52 (1974) 1158–1164, https://doi.org/10.1007/BF0146673434.

[25] A. Madu, C. Cioffe, U. Mian, M. Burroughs, E. Tuomanen, M. Mayers, E. Schwartz, M. Miller, Pharmacokinetics of fluconazole in cerebrospinal fluid and serum of rabbits: validation of an animal model used to measure drug concentrations in cerebrospinal fluid, Antimicrob. Agents Chemother. 38 (1994) 2111–2115, https://doi.org/10.1128/AAC.38.9.2111.

[26] M.G. dosSantos, J.R. Gomes, M.D.M. Costa, Methods used to achieve different levels of the neuronal differentiation process in SH-SY5Y and Neuro2a cell lines: an integrative review, Cell Biol. Int. 47 (2023) 1883–1894, https://doi.org/10.1002/cbin.12093.

[27] S. Chen, W. Samuel, R.N. Fariss, T. Duncan, R.K. Kutty, B. Wiggert, Differentiation of human retinal pigment epithelial cells into neuronal phenotype by N-(4-hydroxyphenyl)retinamide, J. Neurochem. 84 (5) (2003) 972–981, https://doi.org/10.1046/j.1471-4159.2003.

[28] G. Repetto, A. Del Peso, J.L. Zurita, Neutral red uptake assay for the estimation of cell viability/cytotoxicity, Nat. Protoc. 3 (2008) 1125–1131, https://doi.org/10.1038/nprot.2008.75.

[29] H. Wang, J.A. Joseph, Quantifying cellular oxidative stress by dichlorofluorescein assay using microplate reader, Free Radic. Biol. Med. 27 (1999) 612–616, https://doi.org/10.1016/s0891-5849(99)00107-0.

[30] L.A. Lerin, G. Botti, A. Dalpiaz, A. Bianchi, L. Ferraro, C. Chaibi, F. Zappaterra, D. Meola, P.P. Giovannini, B. Pavan, Characterization and hydrolysis studies of a prodrug obtained as ester conjugate of geraniol and ferulic acid by enzymatic way, Int. J. Mol. Sci. 25 (2024) 6263, https://doi.org/10.3390/ijms25116263.

[31] E. Dellera, M.C. Bonferoni, G. Sandri, S. Rossi, F. Ferrari, C. Del Fante, C. Perotti, P. Grisoli, C. Caramella, Development of chitosan oleate ionic micelles loaded with

silver sulfadiazine to be associated with platelet lysate for application in wound healing, Eur. J. Pharm. Biopharm. 88 (2014) 643–650, https://doi.org/10.1016/j.ejpb.2014.07.015.
[32] P.S. Moorhead, Human tumor cell line with a quasi-diploid karyotype (RPMI 2650), Exp. Cell Res. 39 (1965) 190–196, https://doi.org/10.1016/0014-4827(65)90022-4.
[33] E. Esposito, L. Ravani, C. Contado, A. Costenaro, M. Drechsler, D. Rossi, E. Menegatti, A. Grandini, R. Cortesi, Clotrimazole nanoparticle gel for mucosal administration, Mater. Sci. Eng., C 33 (2013) 411–418, https://doi.org/10.1016/j.msec.2012.09.007.
[34] H.P. Erickson, Size and shape of protein molecules at the nanometer level determined by sedimentation, gel filtration, and electron microscopy, Biol. Proced. Online 11 (2009) 32–51, https://doi.org/10.1007/s12575-009-9008-x.
[35] M.P. van den Berg, S.G. Romeijn, J.C. Verhoef, F.W. Merkus, Serial cerebrospinal fluid sampling in a rat model to study drug uptake from the nasal cavity, J. Neurosci. Methods 116 (2002) 99–107, https://doi.org/10.1016/s0165-0270(02)00033-x.
[36] A. Dalpiaz, L. Ferraro, D. Perrone, E. Leo, V. Iannuccelli, B. Pavan, G. Paganetto, S. Beggiato, S. Scalia, Brain uptake of a Zidovudine prodrug after nasal administration of solid lipid microparticles, Mol. Pharm. 11 (2014) 1550–1561, https://doi.org/10.1021/mp400735c.
[37] S. Simovic, P. Heard, H. Hui, Y. Song, F. Peddie, A.K. Davey, A. Lewis, T. Rades, C. A. Prestidge, Dry hybrid lipid-silica microcapsules engineered from submicron lipid droplets and nanoparticles as a novel delivery system for poorly soluble drugs, Mol. Pharm. 6 (2009) 861–872, https://doi.org/10.1021/mp900063t.
[38] B. Neises, W. Steglich, Simple method for the esterification of carboxylic acids, Angew. Chem. Int. Ed. 17 (1978) 522–524, https://doi.org/10.1002/anie.197805221.
[39] L. Wigman, T. Remarchuk, S. Gomez, A. Kumar, M. Dong, M. Michael, C.D. Medley, N. Chetwyn, Byproducts of commonly used coupling reagents: origin, toxicological evaluation and methods for determination, Am. Pharm. Rev. 17 (2014) 6557–6602.
[40] A. Namsi, T. Nury, H. Hamdouni, A. Yammine, A. Vejux, D. Vervandier-Fasseur, N. Latruffe, O. Masmoudi-Kouki, G. Lizard, Induction of neuronal differentiation of murine N2a cells by two polyphenols present in the mediterranean diet mimicking neurotrophins activities: resveratrol and apigenin, Diseases 6 (2018) 67, https://doi.org/10.3390/diseases6030067.
[41] S. Raposo-Garcia, A. Cao, C. Costas, M.C. Louzao, N. Vilariño, C. Vale, L.M. Botana, Mouse N2a neuroblastoma assay: uncertainties and comparison with alternative cell-based assays for ciguatoxin detection, Mar. Drugs 21 (2023) 590, https://doi.org/10.3390/md21110590.
[42] P.S. Williams, Theoretical principles of field-flow fractionation and SPLITT fractionation, in: C. Contado (Ed.), Particle Separation Techniques: Fundamentals, Instrumentation, and Selected Applications (Handbooks in Separation Science), Elsevier Inc., Amsterdam, 2022, pp. 579–620, https://doi.org/10.1016/B978-0-323-85486-3.00001-9.
[43] E. Ghanbari, S.J. Picken, J.H. van Esch, Analysis of differential scanning calorimetry (DSC): determining the transition temperatures, and enthalpy and heat capacity changes in multicomponent systems by analytical model fitting, J. Therm. Anal. Calorim. 148 (2023) 12393–12409, https://doi.org/10.1007/s10973-023-12356-1.
[44] Ü. Gönüllü, M. Üner, G. Yener, E.F. Karaman, Z. Aydoğmuş, Formulation and characterization of solid lipid nanoparticles, nanostructured lipid carriers and nanoemulsion of lornoxicam for transdermal delivery, Acta Pharm. 65 (2015) 1–13, https://doi.org/10.1515/acph-2015-0009.
[45] S.M. Razavi, N. Esmaealzadeh, M. Ataei, N. Afshari, M. Saleh, Y. Amini, S. Hasrati, F. Ghazizadeh Hashemi, A. Mortazavi, L. Mohaghegh Shalmani, A. H. Abdolghaffari, The effects of ursodeoxycholic acid on Parkinson's disease, a mechanistic review of the recent evidence, Metab. Brain Dis. 40 (2025) 115, https://doi.org/10.1007/s11011-025-01542-9.
[46] E. de Oliveira Silva, R. Batista, Ferulic acid and naturally occurring compounds bearing a feruloyl moiety: a review on their structures, occurrence, and potential health benefits, Compr. Rev. Food Sci. Food Saf. 16 (2017) 580–616, https://doi.org/10.1111/1541-4337.12266.
[47] E. Anis, M.F. Zafeer, F. Firdaus, S.N. Islam, A. Anees Khan, A. Ali, M.M. Hossain, Ferulic acid reinstates mitochondrial dynamics through PGC1α expression modulation in 6-hydroxydopamine lesioned rats, Phytother Res. 34 (2020) 214–226, https://doi.org/10.1002/ptr.6523.
[48] G. Cenini, A. Lloret, R. Cascella, Oxidative stress in neurodegenerative diseases: from a mitochondrial point of view, Oxid. Med. Cell. Longev. 2019 (2019) 2105607, https://doi.org/10.1155/2019/2105607.
[49] J. Zhang, M.L. Culp, J.G. Craver, V. Darley-Usmar, Mitochondrial function and autophagy: integrating proteotoxic, redox, and metabolic stress in Parkinson's disease, J. Neurochem. 144 (2018) 691–709, https://doi.org/10.1111/jnc.14308.
[50] G. Botti, L. Catenacci, A. Dalpiaz, L. Randi, M.C. Bonferoni, S. Perteghella, S. Beggiato, L. Ferraro, B. Pavan, M. Sorrenti, Nasal administration of a nanoemulsion based on methyl ferulate and eugenol encapsulated in chitosan oleate: uptake studies in the central nervous system, Pharmaceutics 17 (2025) 367, https://doi.org/10.3390/pharmaceutics17030367.
[51] A. Dalpiaz, B. Cacciari, M. Mezzena, M. Strada, S. Scalia, Solid lipid microparticles for the stability enhancement of a dopamine prodrug, J. Pharm. Sci. 99 (2010) 4730–4737, https://doi.org/10.1002/jps.22178.
[52] A. Dalpiaz, E. Leo, F. Vitali, B. Pavan, A. Scatturin, F. Bortolotti, S. Manfredini, E. Durini, F. Forni, B. Brina, M.A. Vandelli, Development and characterization of biodegradable nanospheres as delivery systems of anti-ischemic adenosine derivatives, Biomaterials 26 (11) (2005) 1299–1306, https://doi.org/10.1016/j.biomaterials.2004.04.033.
[53] J. Rautio, H. Kumpulainen, T. Heimbach, R. Oliyai, D. Oh, T. Järvinen, J. Savolainen, Prodrugs: design and clinical applications, Nat. Rev. Drug Discov. 7 (3) (2008) 255–270, https://doi.org/10.1038/nrd2468.
[54] A. Nudelman, Mutual prodrugs – Codrugs, Curr. Med. Chem. 30 (38) (2023) 4283–4339, https://doi.org/10.2174/0929867330666221209102650.
[55] G. Cásedas, F. Les, C. Choya-Foces, M. Hugo, V. López, The metabolite Urolithin-A ameliorates oxidative stress in Neuro-2a cells, becoming a potential neuroprotective agent, Antioxidants 9 (2) (2020) 177, https://doi.org/10.3390/antiox9020177.
[56] Y. Li, C. Liu, Y. Zhang, S. Mi, N. Wang, Pharmacokinetics of ferulic acid and potential interactions with Honghua and clopidogrel in rats, J. Ethnopharmacol. 137 (2011) 562–567, https://doi.org/10.1016/j.jep.2011.06.011.
[57] S. Manfredini, S. Vertuani, B. Pavan, F. Vitali, M. Scaglianti, F. Bortolotti, C. Biondi, A. Scatturin, P. Prasad, A. Dalpiaz, Design, synthesis and in vitro evaluation on HRPE cells of ascorbic and 6-bromoascorbic acid conjugates with neuroactive molecules, Bioorg. Med. Chem. 12 (2004) 5453–5463, https://doi.org/10.1016/j.bmc.2004.07.043.
[58] A. Dalpiaz, B. Pavan, S. Vertuani, F. Vitali, M. Scaglianti, F. Bortolotti, C. Biondi, A. Scatturin, S. Tanganelli, L. Ferraro, G. Marzola, P. Prasad, S. Manfredini, Ascorbic and 6-Br-ascorbic acid conjugates as a tool to increase the therapeutic effects of potentially central active drugs, Eur. J. Pharm. Sci. 24 (2005) 259–269, https://doi.org/10.1016/j.ejps.2004.10.014.
[59] B. Pavan, A. Dalpiaz, Prodrugs and endogenous transporters: are they suitable tools for drug targeting into the central nervous system? Curr. Pharm. Des. 17 (2011) 3560–3576, https://doi.org/10.2174/138161211798194486.
[60] S.K. Adla, H. Virtanen, T. Thongsodsaeng, K.M. Huttunen, Amino acid transporters in neurological disorders and neuroprotective effects of cysteine derivatives, Neurochem. Int. 177 (2024) 105771, https://doi.org/10.1016/j.neuint.2024.105771.
[61] J. Tampio, A. Králová, S. Riihioja, S. Pitkänen, M. Markowicz-Piasecka, O. Ihamäki, K. Savolainen, S.T. Torunoglu, A.J. Jalkanen, M. Lehtonen, A. Kauppinen, J. Rysä, K.M. Huttunen, Amino acid prodrug of capsaicin improves pharmacokinetic properties in the mouse brain and pancreas, Eur. J. Pharm. Biopharm. 18 (2025) 114797, https://doi.org/10.1016/j.ejpb.2025.114797.
[62] A. Dalpiaz, G. Paganetto, B. Pavan, M. Fogagnolo, A. Medici, S. Beggiato, D. Perrone, Zidovudine and ursodeoxycholic acid conjugation: design of a new prodrug potentially able to bypass the active efflux transport systems of the central nervous system, Mol. Pharm. 9 (2012) 957–968, https://doi.org/10.1021/mp200565g.
[63] N. Agrawal, J. Rowe, J. Lan, Q. Yu, C.A. Hrycyna, J. Chmielewski, Potential tools for eradicating HIV reservoirs in the brain: development of Trojan horse prodrugs for the inhibition of P-glycoprotein with anti-HIV-1 activity, J. Med. Chem. 63 (2020) 2131–2138, https://doi.org/10.1021/acs.jmedchem.9b00779.
[64] H.A. Namanja, D. Emmert, D.A. Davis, C. Campos, D.S. Miller, C.A. Hrycyna, J. Chmielewski, Toward eradicating HIV reservoirs in the brain: inhibiting P-glycoprotein at the blood-brain barrier with prodrug abacavir dimers, J. Am. Chem. Soc. 134 (2012) 2976–2980, https://doi.org/10.1021/ja206867t.
[65] L. Illum, Transport of drugs from the nasal cavity to the central nervous system, Eur. J. Pharm. Sci. 11 (2000) 1–18, https://doi.org/10.1016/s0928-0987(00)00087-7.
[66] F. Erdő, L.A. Bors, D. Farkas, Á. Bajza, S. Gizurarson, Evaluation of intranasal delivery route of drug administration for brain targeting, Brain Res. Bull. 143 (2018) 155–170, https://doi.org/10.1016/j.brainresbull.2018.10.009.
[67] K.M. Huttunen, Improving drug delivery to the brain: the prodrug approach, Expert Opin. Drug Deliv. 21 (2024) 683–693, https://doi.org/10.1080/17425247.2024.2355180.
[68] M.H. Aburahma, S.M. Badr-Eldinm, Compritol 888 ATO: a multifunctional lipid excipient in drug delivery systems and nanopharmaceuticals, Expert Opin. Drug Deliv. 11 (2014) 1865–1883, https://doi.org/10.1517/17425247.2014.935335.
[69] H. Abbas, H. Refai, N. El Sayed, Superparamagnetic Iron oxide-loaded lipid nanocarriers incorporated in thermosensitive in situ gel for magnetic brain targeting of clonazepam, J. Pharm. Sci. 107 (8) (2018) 2119–2127, https://doi.org/10.1016/j.xphs.2018.04.007.
[70] N.R. Abdol Wahab, M.M.R. Meor Mohd Affandi, S. Fakurazi, E. Alias, H. Hassan, Engineering optimized nanostructured lipid carriers for astaxanthin: a response surface methodology approach, Int. J. Nanomedicine. 20 (2025) 15515–15529, https://doi.org/10.2147/IJN.S544064.
[71] F. Han, S. Li, R. Yin, H. Liu, L. Xu, Effect of surfactants on the formation and characterization of a new type of colloidal drug delivery system: nanostructured lipid carriers, Colloids Surf. A Physicochem. Eng. Asp. 315 (2008) 210–216, https://doi.org/10.1016/j.colsurfa.2007.08.005.
[72] K.O. Kullavadee, R. Uracha, S.M. Smith, Effect of surfactant on characteristics of solid lipid nanoparticles (SLN), Adv. Mater. Res. 364 (2012) 313–316. https://doi.org/10.4028/www.scientific.net/AMR.364.313.
[73] A. Dalpiaz, M. Fogagnolo, L. Ferraro, S. Beggiato, M. Hanuskova, E. Maretti, F. Sacchetti, E. Leo, B. Pavan, Bile salt-coating modulates the macrophage uptake of nanocores constituted by a zidovudine prodrug and enhances its nose-to-brain delivery, Eur. J. Pharm. Biopharm. 144 (2019) 91–100, https://doi.org/10.1016/j.ejpb.2019.09.008.
[74] N. Washington, R.J.C. Steele, S.J. Jackson, D. Bush, J. Mason, D.A. Gill, K. Pitt, D. A. Rawlins, Determination of baseline human nasal pH and the effect of intranasally administered buffers, Int. J. Pharm. 198 (2) (2000) 139–146, https://doi.org/10.1016/S0378-5173(99)00442-1.

[75] A. Clementino, M. Batger, G. Garrastazu, M. Pozzoli, E. Del Favero, V. Rondelli, B. Gutfilen, T. Barboza, M.B. Sukkar, S.A.L. Souza, L. Cantù, F. Sonvico, The nasal delivery of nanoencapsulated statins - an approach for brain delivery, Int. J. Nanomedicine. 11 (2016) 6575–6590, https://doi.org/10.2147/IJN.S119033.
[76] Z. Shengnan, T. Le, N. Davies, R. Löbenberg, Development of a physiologically relevant simulated nasal fluid for in vitro dissolution studies, Dissolution Technol. 32 (2025) 20–31, https://doi.org/10.14227/DT320125P20.
[77] S. Amézqueta, U. Casanova, E. Fuguet, C. Ràfols, Estimation of the critical micelle concentration of sodium taurocholate in intestine-relevant conditions using complimentary techniques, Microchem. J. 214 (2025) 113934, https://doi.org/10.1016/j.microc.2025.113934.
[78] C. Viegas, A.B. Patrício, J.M. Prata, A. Nadhman, P.K. Chintamaneni, P. Fonte, Solid lipid nanoparticles vs. nanostructured lipid carriers: a comparative review, Pharmaceutics 15 (6) (2023) 1593, https://doi.org/10.3390/pharmaceutics15061593.
[79] G. Botti, A. Dalpiaz, B. Pavan, Targeting systems to the brain obtained by merging prodrugs, nanoparticles, and nasal administration, Pharmaceutics 13 (2021) 1144, https://doi.org/10.3390/pharmaceutics13081144.
[80] X. Gao, Y. Xiong, H. Chen, X. Gao, J. Dai, Y. Zhang, W. Zou, Y. Gao, Z. Jiang, B. Han, Mucus adhesion vs. mucus penetration? Screening nanomaterials for nasal inhalation by MD simulation, J. Contr. Release 353 (2023) 366–379, https://doi.org/10.1016/j.jconrel.2022.11.051.
[81] M.A. Mirza, A.K. Panda, S. Asif, D. Verma, S. Talegaonkar, N. Manzoor, A. Khan, F. J. Ahmed, M. Dudeja, Z. Iqbal, A vaginal drug delivery model, Drug Deliv. 23 (8) (2016) 3123–3134, https://doi.org/10.3109/10717544.2016.1153749.
[82] H.A. Abou-Taleb, Z. Fathalla, D.M. Naguib, A.A. Fatease, H. Abdelkader, Chitosan/solid-lipid nanoparticles hybrid gels for vaginal delivery of estradiol for management of vaginal menopausal symptoms, Pharmaceuticals 16 (9) (2023) 1284, https://doi.org/10.3390/ph16091284.